

Self-Contrastive Forward-Forward Algorithm

Xing Chen^{1*}, Dongshu Liu¹, Jérémie Laydevant^{2,3}, Julie Grollier^{1*}

^{1*}Laboratoire Albert Fert, CNRS, Thales, Université Paris-Saclay, 1 av.
A. Fresnel, Palaiseau, 91767, France.

²School of Applied and Engineering Physics, Cornell University, Ithaca,
NY 14853, USA.

³USRA Research, Institute for Advanced Computer Science, Mountain
View, CA 94035, USA.

*Corresponding author(s). E-mail(s): xing.chen@cnrs-thales.fr;
julie.grollier@cnrs-thales.fr;

Contributing authors: dongshu.liu@cnrs.fr;
jeremie.laydevant@gmail.com;

Abstract

The Forward-Forward (FF) algorithm is a recent, purely forward-mode learning method, that updates weights locally and layer-wise and supports supervised as well as unsupervised learning. These features make it ideal for applications such as brain-inspired learning, low-power hardware neural networks, and distributed learning in large models. However, while FF has shown promise on written digit recognition tasks, its performance on natural images and time-series remains a challenge. A key limitation is the need to generate high-quality negative examples for contrastive learning, especially in unsupervised tasks, where versatile solutions are currently lacking. To address this, we introduce the Self-Contrastive Forward-Forward (SCFF) method, inspired by self-supervised contrastive learning. SCFF generates positive and negative examples applicable across different datasets, surpassing existing local forward algorithms for unsupervised classification accuracy on MNIST (MLP: 98.7%), CIFAR-10 (CNN: 80.75%), and STL-10 (CNN: 77.3%). Additionally, SCFF is the first to enable FF training of recurrent neural networks, opening the door to more complex tasks and continuous-time video and text processing.

Keywords: Local learning, Self-supervised learning, Unsupervised learning, Contrastive learning, Neuromorphic Computing

1 Introduction

Purely-forward and local algorithms propagate signals from inputs to outputs, without any backward pass, and employ a learning rule that is local in space, using signals only from pre- and post- neurons to update a weight. These algorithms, which include well-known Hebbian learning methods [1], have long been studied to model the brain, as their features align with biological processes, contrarily to error backpropagation [2]. They are also ideal for on-chip learning of low-power embedded hardware. The purely forward architecture addresses the challenge of implementing backpropagation on neuromorphic chips, a key obstacle that has been limiting the development of on-chip training for these systems [3]. The local learning rule allows synaptic devices to be directly updated by signals from neuron devices, eliminating the need to store neural activations for gradient computation, thus significantly reducing memory usage, power consumption as well as training times [4].

The practical application of these algorithms was historically limited by low accuracy on deep learning image recognition benchmarks, such as CIFAR-10 (labeled) and STL-10 (unlabeled). However, in recent years, accuracy has significantly improved thanks to their integration with automatic differentiation tools and activation functions, combined with the use of standardization and pruning techniques [5–14]. As a result, these algorithms have become relevant not only for brain modeling and energy-efficient training of neuromorphic chips, but also for distributed learning of large-scale models across multiple devices [15–18].

These advances have motivated the recent development of novel purely forward and local algorithms aimed at improving accuracy and simplifying implementation for various applications. The Forward-Forward (FF) algorithm is a key example of this new breed of algorithms [19]. Its main advantages are its simplicity and versatility, allowing it in principle to handle both unsupervised and supervised learning, and to process time-series as well as static inputs — while many other purely forward and local algorithms are limited to a single category. As a result, the FF algorithm has attracted significant interest since its introduction [7, 20–27], inspiring variants with improved accuracy and architectures and addressing tasks such as image recognition, temporal sequence classification, and reinforcement learning [14, 28–39]. Early demonstrations of FF *in silico* already cover a wide range of hardware platforms, including microcontrollers [40], in-memory computing systems utilizing Vertical NAND Flash Memory as synapses [41], and physical implementations where neurons are replaced by acoustic, optical, or microwave technologies [42, 43].

Fig 1 highlights recent advancements in the Forward-Forward algorithm (FF, shown in purple) [14, 19, 33, 38], comparing its accuracy on image classification tasks with algorithms that are also both purely forward and local (shown in black [5–14]). As illustrated, the accuracy of FF supervised training has significantly improved from below 60% [19] to 88.2% recently [44], progressively catching up with the best supervised, purely local, and forward algorithm [5]. In unsupervised learning, where FF’s greatest potential for on-chip training may lie, it has only achieved high accuracy on the MNIST task [19, 45], with limited [38] or no success on more challenging datasets such as CIFAR-10 [46] or STL-10 [47].

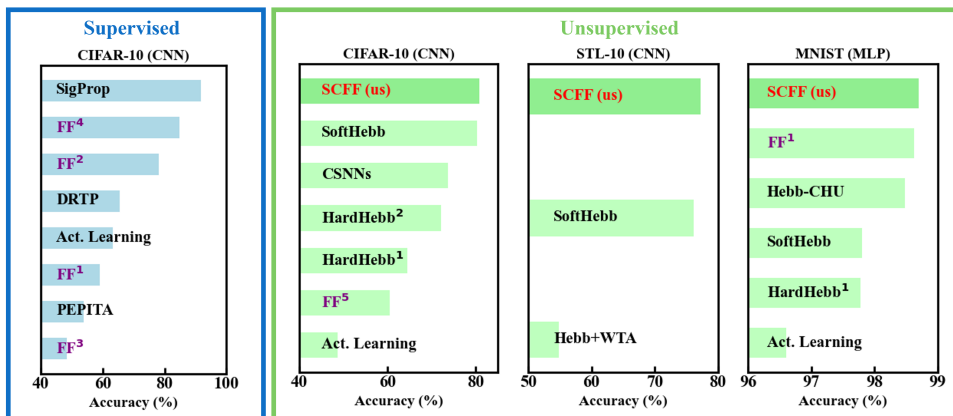


Fig. 1: Comparison of algorithms that are both purely forward and local across different tasks. The blue frame displays the CIFAR-10 results achieved by various supervised local learning methods. The green frame presents the results of different local and unsupervised learning methods on CIFAR-10, STL-10, and MNIST datasets, respectively. Algorithms related to FF are highlighted in purple. FF¹ refers to [19], FF² to [33], FF³ to [14], FF⁴ to [44], and FF⁵ to [38]. Our method, SCFF, is indicated in red. SigProp refers to [5], DRTP to [6], Act.Learning to [7], PEPITA to [8], SoftHebb to [9], CSNNs to [10], HardHebb² to [12], HardHebb¹ to [11], Hebb+WTA to [9] and Hebb-CHU to [13].

Inspired by the noise contrastive estimation (NCE) method [48], the Forward-Forward (FF) algorithm presents positive and negative examples sequentially to the network inputs. Once trained, the network is expected to produce distinctly different neural responses across all layers for these examples. The key challenge is generating “negative” examples that closely resemble the training data but still provide enough contrast for the network to learn meaningful representations.

Supervised learning methods applicable to any dataset have been developed, solving tasks like MNIST and CIFAR-10 [19, 32]. However, for unsupervised FF learning, there is no universal method to generate positive and negative examples for all databases, hindering FF’s application to more complex unsupervised tasks beyond MNIST. This limitation is evident in the few FF points in the Unsupervised panel of Fig 1, where only Hebbian and activation learning algorithms have successfully solved CIFAR-10 and STL-10 by combining a local rule with a purely forward architecture.

Moreover, the FF algorithm currently lacks the ability to handle time-varying sequential data, limiting its applicability in neuromorphic systems which often deal with dynamic inputs from the real world. While the original FF paper [19] includes a multi-layer recurrent neural network, its purpose is to model top-down effects, using a static MNIST image repeated over time frames as input. Another implementation demonstrates a limited form of sequence learning with a fully connected network,

but this architecture could not handle real-time sequential data due to the absence of recurrence. As a result, FF has yet to be extended to effectively handle recurrent network scenarios for time-varying inputs.

In this work, we introduce the Self-Contrastive Forward-Forward (SCFF) method, where each data sample is contrasted within itself to enable efficient learning. This method is inspired by self-supervised learning to provide a simple and effective way to generate positive and negative examples for any dataset. In SCFF, a positive example is created by concatenating an input with itself, while a negative example is formed by concatenating the input with a randomly selected example from the training set. This simple method (red points in Fig 1) not only extends the capabilities of FF to unsupervised tasks but also surpasses the state-of-the-art accuracy of similar algorithms on the MNIST, CIFAR-10, and STL-10 image datasets. It also opens the path to solving sequential tasks by contrasting inputs with FF. More specifically, our contributions are:

- We propose an approach called SCFF that takes inspiration from self-supervised learning to generate positive and negative examples and train neural networks with the Forward-Forward algorithm in an unsupervised way, applicable to a wide range of databases.
- We show that SCFF significantly outperforms existing unsupervised purely-Forward and local learning algorithms in image classification tasks. With a multilayer perceptron (MLP), we achieved a test accuracy of 98.7% on MNIST. With a convolutional neural network (CNN), we reached 80.75% on CIFAR-10 and 77.3% STL-10 (which includes a small number of labeled examples alongside a much larger set of unlabeled data).
- We present the first demonstration of the FF approach being successfully applied to sequential data. Our findings show that the proposed SCFF method effectively learns representations from time-varying sequential data using a recurrent neural network. In the Free Spoken Digit Dataset (FSDD), SCFF training results in an accuracy improvement of over 10 percentage points compared to scenarios where hidden connections remain untrained (random).
- We conduct a theoretical and illustrative analysis of the distribution of negative examples generated with our method in comparison to positive examples within the data space. The analysis reveals that negative data points consistently position themselves between distinct clusters of positive examples. This positioning suggests that negative examples play a crucial role in pushing apart and further separating adjacent positive clusters, thereby enhancing the efficiency of classification.

Our results demonstrate the potential of Self-Contrastive Forward-Forward (SCFF) methods for efficient and flexible layer-wise learning of useful representations in a local and purely forward unsupervised manner. In section 2.1 and 2.2, we will introduce the two foundational methods that SCFF builds upon: the original Forward-Forward algorithm and Contrastive Self-Supervised learning, highlighting their differences and similarities. Next, in section 3, we will present our Contrastive Forward-Forward algorithm and discuss our findings. Finally, we will explore the relationship of SCFF to other purely forward and/or local learning methods in the discussion of section 4.

2 Background

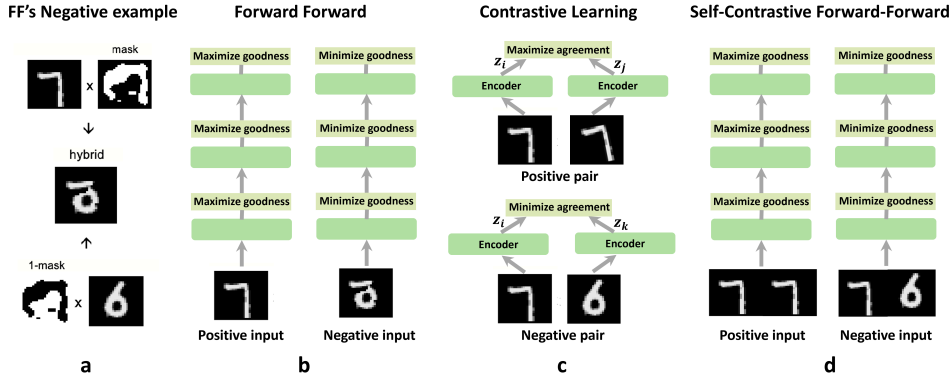


Fig. 2: Comparative diagram illustrating three distinct unsupervised (self-supervised) learning paradigms. **a.** Generation of a negative example is implemented by hybridization of two different images in the original FF paper [19]. **b.** In Forward Forward (FF) Learning, the layer-wise loss function is defined so as to maximize the goodness for positive inputs (real images) and minimize the goodness for negative inputs, each of which is generated by corrupting the real image to form a fake image, as shown in **a**. **c.** In Contrastive Learning, the InfoNCE loss function determines the similarity between representations of two inputs (two different inputs or two same inputs but with different augmentations) in the end of the network [49]. **d.** Our proposed Contrastive Forward Forward Learning algorithm combines the principles of Forward Forward Learning and Contrastive Learning algorithms to maximize the goodness for concatenated similar pairs and minimize the goodness for dissimilar pairs with a layer-wise loss function.

2.1 The original Forward-Forward algorithm

The original Forward-Forward algorithm is depicted in Fig 2b. For an input example \mathbf{x}_i , each layer's output is assigned a 'goodness' score $G_i^{(l)}$, where l is the layer index. This score is calculated as the mean of the squared activities of the output neurons at layer l : $G_i^{(l)} = \frac{1}{M^{(l)}} \sum_m y_{i,m}^2$, where $M^{(l)}$ is the number of neurons at layer l and m represents the neuron index.

Predefined positive and negative examples are successively presented to the network's input. The possibility of a positive example \mathbf{x}_i being recognized as positive and a negative example \mathbf{x}_j being recognized as negative by the network are defined as $p_{\text{pos}}(\mathbf{x}_i) = \sigma(G_i^{(l)} - \Theta_{\text{pos}}^{(l)})$ and $p_{\text{neg}}(\mathbf{x}_j) = \sigma(\Theta_{\text{neg}}^{(l)} - G_j^{(l)})$ respectively. The sigmoid function $\sigma(x) = \frac{1}{1+e^{-x}}$ evaluates the effectiveness of the separation, where $\Theta_{\text{pos}}^{(l)}$ and $\Theta_{\text{neg}}^{(l)}$ are fixed values that serve as hyperparameters of the network.

Inspired by Noise-Contrastive Estimation [48], which aims to distinguish positive examples from noisy examples, the objective of FF learning is to increase the goodness score for positive input examples so that it significantly exceeds the threshold ($p_{\text{pos}}(\mathbf{x}_i) \rightarrow 1$) and to decrease the goodness score for negative input examples so that it falls well below the threshold ($p_{\text{neg}}(\mathbf{x}_j) \rightarrow 1$). Weight updates are performed locally by combining the gradients derived from both positive and negative examples:

$$\begin{aligned} \mathcal{L}_{\text{FF}} &= -\mathbb{E}_{\mathbf{x}_i \sim \text{pos}} \log p_{\text{pos}}(\mathbf{x}_i) - \mathbb{E}_{\mathbf{x}_j \sim \text{neg}} \log p_{\text{neg}}(\mathbf{x}_j) \\ &= -\mathbb{E}_{G_{i,\text{pos}}^{(l)}} \left[\log \sigma(G_{i,\text{pos}}^{(l)} - \Theta_{\text{pos}}^{(l)}) \right] - \mathbb{E}_{G_{j,\text{neg}}^{(l)}} \left[\log \sigma(\Theta_{\text{neg}}^{(l)} - G_{j,\text{neg}}^{(l)}) \right] \end{aligned} \quad (1)$$

where $G_{i,\text{pos}}^{(l)}$ and $G_{i,\text{neg}}^{(l)}$ respectively correspond to the goodness for the positive and negative examples input at layer l . The final loss is computed over all N examples in the batch.

Hinton [19] proposed that FF can be used for self-supervised representation learning by using real data vectors as the positive examples and engineered data vectors as the negative examples. The negative examples should be carefully designed, rather than relying on random corruption methods of the training data like noise injection or occlusion. The negative data needs to be sufficiently challenging to ensure the network learns useful information. To make FF focus on the long-range correlations in images that characterize shapes, the negative data should have very different long-range correlations while maintaining similar short-range correlations. For the MNIST dataset, this can be achieved by creating a mask with large regions of ones and zeros. As proposed in the original framework [19], negative data is then generated by combining one digit image multiplied by the mask with a different digit image multiplied by the inverse of the mask, as illustrated in Fig 2a. Although this method performs well for MNIST (as shown in the Unsupervised panel in Fig 1), it does not easily translate to more complex image databases like CIFAR-10 and STL-10, resulting in limited accuracy on these benchmarks.

2.2 Contrastive self-supervised learning

In this article, we draw inspiration from contrastive self-supervised learning methods to construct positive and negative examples for FF, applicable to any image database and beyond. Contrastive learning, illustrated in Fig 2c, is a self-supervised technique designed to learn representations by contrasting positive pairs against negative pairs. This approach relies heavily on data augmentation, where a positive pair consists of two different augmented views of the same data sample, and negative pairs are constructed from different samples. While FF shares strong similarities with contrastive learning, it also has key differences.

Both methods utilize the concept of contrasting positive and negative examples to guide the learning process. They also both aim to learn meaningful data representations without labeled data in the first phase, allowing to extract information from the hidden layers in the second phase by training a linear classifier.

However, their loss functions are fundamentally different. FF focuses on the absolute goodness of positive versus negative examples, decoupling them in the loss. On the other hand, general contrastive losses employ relative comparisons through distances or similarities between positive and negative examples.

Additionally, the neural network optimization method differs. FF defines a local loss function at each layer and avoids backpropagation through hidden layers, whereas typical contrastive learning approaches train deep networks end-to-end. Lastly, self-supervised FF emphasizes data corruption to generate negative examples, focusing on specific characteristics of corruption to enhance learning, while contrastive learning relies heavily on varied data augmentation techniques.

3 Self-Contrastive Forward-Forward algorithm and results

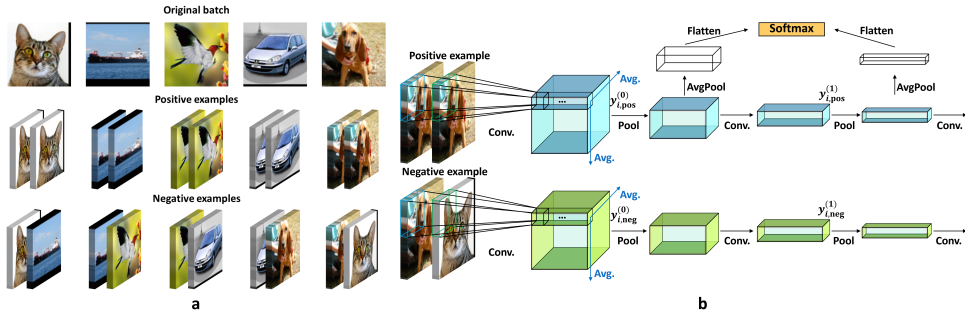


Fig. 3: SCFF method for processing with Convolutional Neural Network Architecture. **a.** The original batch of images (top row) is processed to generate positive (middle row) and negative examples (bottom row). **b.** The generated positive and negative examples undergo a series of convolutional (Conv.) and pooling (AvgPool or Maxpool) operations to extract relevant features. The output neurons which are extracted from each hidden layer after an external average pooling layer are then fed together into a softmax layer for final classification.

We draw inspiration from contrastive self-supervised learning algorithms to propose the Self-Contrastive Forward-Forward (SCFF) algorithm, which addresses the drawbacks of FF, including the complexity of generating negative examples and its inability to generalize well to convolutional neural networks in a purely forward manner.

3.1 Creating the negative and positive examples

Instead of contrasting the representations in the feature space as in contrastive self-supervised learning (Fig 2c), SCFF directly takes pairs of positive and negative images as inputs to the neural network (Fig 2d). More specifically, given a batch of N training examples, and for a randomly selected example \mathbf{x}_k ($k \in \{1, N\}$) in the batch, the positive example $\mathbf{x}_{i,\text{pos}}^{(0)}$ (the number 0 is the layer index) is the concatenation of two repeated \mathbf{x}_k , i.e., $\mathbf{x}_{i,\text{pos}}^{(0)} = [\mathbf{x}_k, \mathbf{x}_k]^T$. The negative example $\mathbf{x}_{j,\text{neg}}^{(0)}$ is obtained by concatenating \mathbf{x}_k with another example \mathbf{x}_n ($n \neq k$) in the batch, i.e., $\mathbf{x}_{j,\text{neg}}^{(0)} = [\mathbf{x}_k, \mathbf{x}_n]^T$ (or $[\mathbf{x}_n, \mathbf{x}_k]^T$). Fig 3a shows some instances of generated positive and negative examples from the original training batch for the STL-10 dataset.

Considering the case of a fully connected network, the concatenated pair of images (positive or negative examples) are sent as inputs to the network. The outputs for the positive and negative examples from the first layer can be written respectively as $\mathbf{y}_{i,\text{pos}}^{(0)} = f(W_1\mathbf{x}_k + W_2\mathbf{x}_k)$, $\mathbf{y}_{j,\text{neg}}^{(0)} = f(W_1\mathbf{x}_k + W_2\mathbf{x}_n)$, where f is the ReLU activation function. The weight matrices W_1 and W_2 correspond to the connections to the two images. In practice, we set $W_1 = W_2$ because the gradient of the loss function with respect to W_1 and W_2 converges to the same value. Setting $W_1 = W_2$ accelerates the training speed and improves the performance. Intuitively, this can be understood by recognizing that swapping the positions of \mathbf{x}_k and \mathbf{x}_n in the concatenated image should not affect the output neural activities. For a rigorous mathematical proof, see Appendix A.

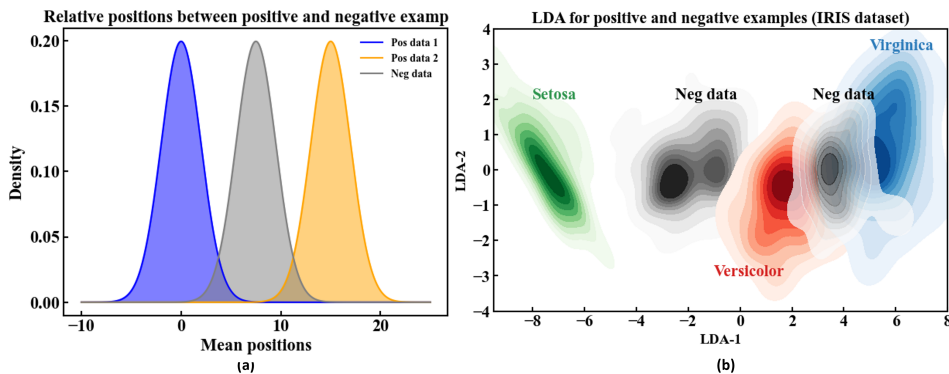


Fig. 4: Probability distributions of relative positions between positive and negative examples. **a** Theoretical distributions of positive examples from two different classes with distinct means ($2\mu_1 = 0$ and $2\mu_2 = 15$) and identical variance ($2\Sigma = 4$) are shown with blue and orange curves, respectively. The theoretical distribution of negative examples derived from the two classes using the formula 2 is depicted by the grey curve. **b** Continuous probability density of LDA applied to the IRIS dataset, displaying contours for positive examples in green, red, and blue, and for negative examples in grey.

The concept of SCFF can be understood through the lens of Noise Contrastive Estimation (NCE). In NCE, a key insight is that “the noise distribution should be close to the data distribution, because otherwise, the classification problem might be too easy and would not require the system to learn much about the structure of the data” [48]. Our method of generating the positive and negative examples aligns with this principle if we treat the negative examples as “noise data”. We assume that the data samples for each class follow a multivariate Gaussian distribution with a shared covariance matrix Σ and that each class is statistically independent of the others—assumptions commonly employed in various statistical models [50]. Furthermore, noting that the input weight matrices W_1 and W_2 are identical, i.e. $W = W_1 = W_2$, the concatenated inputs processed by the network are simplified as follows: the positive example becomes $\mathbf{y}_{i,\text{pos}}^{(0)} = f(W_1\mathbf{x}_k + W_2\mathbf{x}_k) = f(W(2\mathbf{x}_k))$, and the negative example is $\mathbf{y}_{j,\text{neg}}^{(0)} = f(W_1\mathbf{x}_k + W_2\mathbf{x}_n) = f(W(\mathbf{x}_k + \mathbf{x}_n))$. This is equivalent to treating the positive examples as $\mathbf{x}_{i,\text{pos}}^{(0)} = 2\mathbf{x}_k$ and negative examples as $\mathbf{x}_{j,\text{neg}}^{(0)} = \mathbf{x}_k + \mathbf{x}_n$. Therefore, the distributions of positive examples $\mathbf{x}_{i,\text{pos}}^{(0)}$ and negative examples $\mathbf{x}_{j,\text{neg}}^{(0)}$ follow :

$$\begin{aligned}\mathbf{x}_{i,\text{pos}}^{(0)} &\sim \mathcal{N}(2\boldsymbol{\mu}_1, 2\boldsymbol{\Sigma}) \\ \mathbf{x}_{j,\text{neg}}^{(0)} &\sim \mathcal{N}(\boldsymbol{\mu}_1 + \boldsymbol{\mu}_2, 2\boldsymbol{\Sigma})\end{aligned}\tag{2}$$

where $\boldsymbol{\mu}_1$ and $\boldsymbol{\mu}_2$ are means of two different classes respectively. Theoretically, the negative examples always lie somewhere between two different clusters of positive examples in the sample space, as illustrated in Fig. 4a for the one-dimensional case. For practical analysis with a real-world dataset, we visualized the distributions of positive and negative examples from the IRIS dataset [51] using 2D linear discriminant analysis (LDA), which distinguishes between three different types of irises, as shown in Fig. 4b. This visualization shows that the negative examples are positioned between different clusters of positive examples, suggesting that they contribute to pushing apart and further separating adjacent positive examples as they are mapped into higher-dimensional space during training. Additionally, negative examples are formed by combining two examples from different classes, enriching the diversity of negative examples and leading to more robust training. For a detailed analysis of how the LDA components evolve during training as the input data is mapped into the feature space and more theoretical results, please refer to Appendix B.

3.2 Training procedure

We evaluate SCFF on different image datasets including MNIST [45], CIFAR-10 [46] and STL-10 [47] (results in Fig. 1 and Fig. 5), as well as an audio dataset Free Spoken Digit Dataset (FSDD) [52] (results in Fig. 6).

Each layer of the network was fully trained and frozen before training the next one. After unsupervised training with SCFF, we froze the network and trained a linear downstream classifier [9, 53] with the back-propagation method on representations created by the network using the labeled data. The linear classifier was optimized using cross-entropy loss. The accuracy of this classification serves as a measure of the quality

of the learned representations. To ensure successful training and high accuracy in the final model, several important techniques were utilized during the training process. These techniques include the “Triangle” method [11, 47] for transmitting information between layers, adding a penalty term in the loss function to ensure stable training, and applying an extra pooling layer to retrieve information at each layer. For further details, see the Methods section.

All details about the impact of hyperparameters and the training of the linear classifier are provided in Appendix F and G.

3.3 Fully connected network: MNIST

On the MNIST dataset, when trained on a two-layer fully connected network with 2000 hidden neurons each, SCFF achieves a test precision of 98.7%, which is comparable to the performance achieved by backpropagation [19]. This surpasses previously published benchmarks on other biologically inspired algorithms, such as 97.9% in [9], 98.42% in [8] (supervised training), and 96.6% in [7]. The full comparison is shown in the right column of the green frame in Fig 1.

3.4 Convolutional neural networks: CIFAR-10 and STL-10

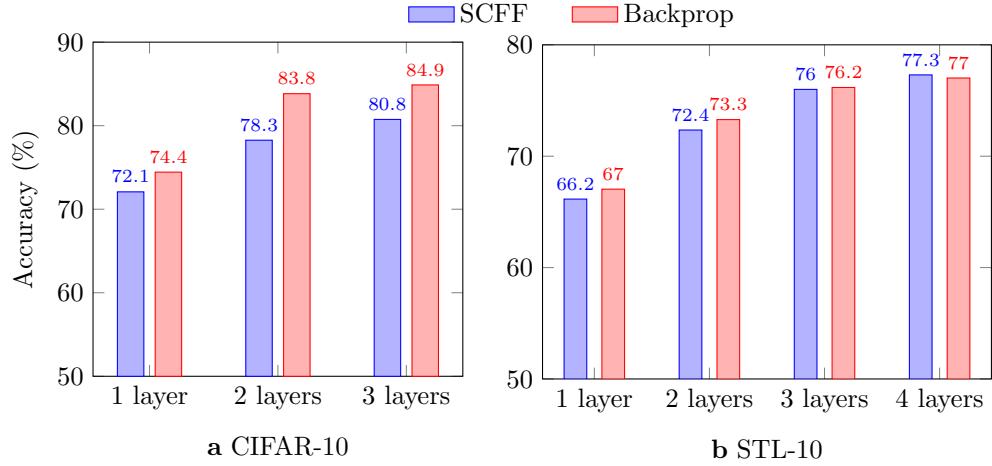


Fig. 5: Comparison of test accuracy at different layers by using SCFF and Backpropagation methods on CIFAR-10 in **a** and on STL-10 dataset in **b**.

The convolutional neural network processes three-dimensional color images. The original images are concatenated along the channel dimension to form positive or negative inputs (see Fig 3). The output of each convolutional layer is represented as a three-dimensional vector $\mathbf{y}_{i,\text{pos}}^{(l)}$ (or $\mathbf{y}_{i,\text{neg}}^{(l)}$) $\in \mathbb{R}^{C \times H \times W}$. The Loss function at layer l is then defined as:

$$\begin{aligned} \mathcal{L}_{\text{SCFF}} = & -\mathbb{E}_{G_{i,\text{pos}}^{(l)}} \left[\frac{1}{H \times W} \sum_h^H \sum_w^W \log \sigma(G_{i,h,w,\text{pos}}^{(l)} - \Theta_{\text{pos}}^{(l)}) \right] \\ & -\mathbb{E}_{G_{j,\text{neg}}^{(l)}} \left[\frac{1}{H \times W} \sum_h^H \sum_w^W \log \sigma(\Theta_{\text{neg}}^{(l)} - G_{j,h,w,\text{neg}}^{(l)}) \right] \end{aligned} \quad (3)$$

where the goodness of neural activities is calculated over the channels as $G_{i,h,w,\text{pos}}^{(l)} = \frac{1}{C} \sum_c y_{i,c,h,w,\text{pos}}^{2(l)}$ (or $G_{i,h,w,\text{neg}}^{(l)} = \frac{1}{C} \sum_c y_{i,c,h,w,\text{neg}}^{2(l)}$).

For the CIFAR-10 and STL-10 datasets, we employed convolutional neural networks with architectures identical to those in [9] to extract features. SCFF achieves a test accuracy of 80.75% with a three-layer convolutional architecture (number of filters each layer: 96-384-1536) on CIFAR-10 and 77.3% with a four-layer convolutional architecture (number of filters each layer: 96-384-1536-6144) on STL-10. These results surpass the previous state-of-the-art accuracies for purely-forward unsupervised learning, of 80.3% on CIFAR-10 and 76.2% on STL-10 achieved using the SoftHebb algorithm [9]. This demonstrates the significant potential of the SCFF method to scale effectively to more complex datasets and architectures. The full comparison is shown in the left column of the green frame in Fig. 1.

We also compared the test accuracies at each layer using SCFF and Backpropagation (BP) methods on CIFAR-10 and STL-10, as shown in 5. Notably, for STL-10, SCFF achieved a final layer performance of 77.3% higher than the one of BP: 77.02%(Fig. 5b). This is because the STL-10 dataset contains a large amount of unlabeled images, which limits the effectiveness of supervised BP training. By fine-tuning SCFF with end-to-end BP on the few labelled STL-10 examples, SCFF’s accuracy further improves to 80.13%. This demonstrates that SCFF is highly suitable for unsupervised pretraining followed by supervised BP training, making it ideal for semi-supervised learning approaches.

Unlike other unsupervised learning methods, where the result is obtained solely from the final layer’s output, SCFF integrates neuron information with the linear classifier from intermediate layers, leading to more comprehensive feature extraction [19]. For CIFAR-10 (Fig. 5 a), the test accuracy for the two-layer and three-layer models was obtained by combining the outputs of all previous layers (pooled information for dimensionality reduction; see Methods section) before feeding them into the final linear classifier. However, because the STL-10 dataset consists of high-quality images, the number of output neurons in each layer is much larger than that in CIFAR-10. Therefore, for the STL-10 dataset, we did not combine outputs from previous layers for training the linear classifier, with the exception of the fourth layer. In this case, we combined the outputs from both the third and fourth layers for the final classification, resulting in a 1% improvement in accuracy compared to using only the fourth layer’s outputs as input to the linear classifier.

By visualizing and investigating the class activation map, which highlights the importance of each region of a feature map in relation to the model’s output, we

can intuitively observe that after four layers, more distinct and meaningful structures emerge (see Appendix H). Specifically, the activation maps corresponding to higher-layer features focus on the general contours and key objects within the input, facilitating improved feature extraction and classification [54].

3.5 Recurrent neural network: FSDD audio dataset

The original FF paper [19] introduces a specialized recurrent neural network (RNN) that models top-down effects using repeated static images as input for each time frame. In contrast, our work focuses on training an RNN that processes time-varying inputs.

We employ the Free Spoken Digit Dataset (FSDD), a standard benchmark task for evaluating RNN training performance [55–57]. The FSDD is a collection of audio recordings where speakers pronounce digits (0-9) in English. We follow the standard procedure consisting in extracting frequency domain information at different time intervals, here through Mel-Frequency Cepstral Coefficient (MFCC) features (39 channels) [58]. Plots of the evolution of MFCC feature with time are shown in Fig. 6 for the digits 3 and 8. The SCFF method forms positive and negative examples by concatenating the same input for positive examples, and different ones for negative examples. Fig. 6a presents a negative example which is generated by concatenating MFCC features from two different digits. The goal of the task is to recognize the digit after feeding in the full sequence, from the output of the network at the last time step.

We train a Bi-directional Recurrent Neural Network (Bi-RNN) in an unsupervised way using the SCFF method to classify the digits. The procedure that we use for this purpose is illustrated in Fig. 6a. Unlike conventional uni-directional RNNs, where sequential input is processed step by step in a single direction, resulting in a sequence of hidden states from H_0 to H_T (as depicted in the bottom RNN in Fig. 6a), the Bi-RNN comprises two RNNs that process the input in parallel in both forward and backward directions. This results in hidden states evolving from H_0 to H_T in the forward RNN and from H_T^* to H_0^* in the backward RNN*, as shown in the top portion of the figure. The red regions in the figure highlight the features at different time steps. This bidirectional structure is particularly advantageous for tasks where context from both preceding and succeeding audio frames is critical, such as speech recognition, enhancing model performance compared to conventional uni-directional RNNs [59].

The output of each directional RNN for a positive or negative input example is a two-dimensional vector $\mathbf{h}_i \in \mathbb{R}^{M \times T}$, where T represents the number of time steps and M denotes the number of hidden neurons. The loss function at layer l is then defined as:

$$\begin{aligned} \mathcal{L}_{\text{SCFF}} = & - \mathbb{E}_{G_{i,\text{pos}}^{(l)}} \left[\frac{1}{T} \sum_t \log \sigma(G_{i,t,\text{pos}}^{(l)} - \Theta_{\text{pos}}^{(l)}) \right] \\ & - \mathbb{E}_{G_{j,\text{neg}}^{(l)}} \left[\frac{1}{T} \sum_t \log \sigma(\Theta_{\text{neg}}^{(l)} - G_{j,t,\text{neg}}^{(l)}) \right] \end{aligned} \quad (4)$$

where the goodness of neural activities is calculated at each time step as $G_{i,t,\text{pos}}^{(l)} = \frac{1}{M} \sum_m h_{i,t,m,\text{pos}}^{2(l)}$ (or $G_{i,t,\text{neg}}^{(l)} = \frac{1}{M} \sum_m h_{i,t,m,\text{neg}}^{2(l)}$).

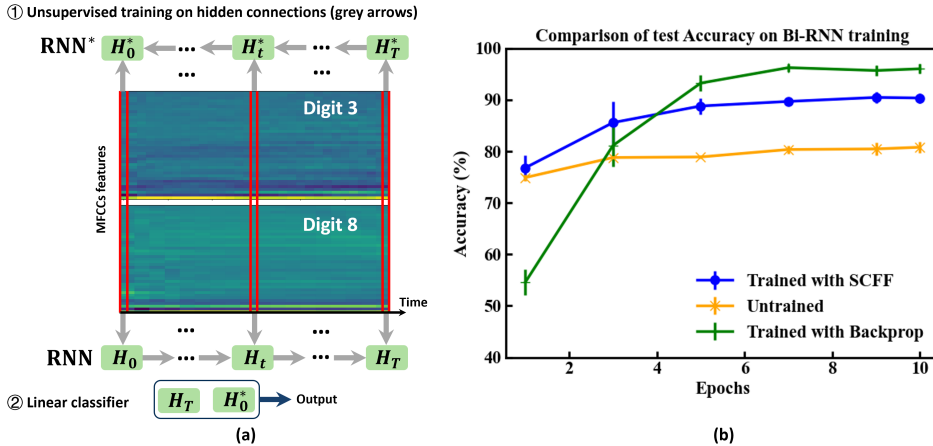


Fig. 6: Bi-directional RNN results on FSDD dataset. **a.** Training procedure of SCFF on a Bi-RNN. In the first stage, unsupervised training is performed on the hidden connections (both input-to-hidden and hidden-to-hidden transformations) using positive and negative examples. Positive examples are created by concatenating two identical MFCC feature vectors of a digit along the feature dimension, while negative examples are generated by concatenating MFCCs from two different digits, as illustrated in the figure. At each time step, the features are sequentially fed into the Bi-RNN (RNN and RNN*). The red regions indicate features at different time steps. In the second stage, a linear classifier is trained using the final hidden states from both RNNs, i.e., H_T and H_0^* as inputs for classification task. **b.** Comparison of test accuracy for the linear classifier trained on Bi-RNN outputs. The yellow curve represents accuracy with untrained (random) hidden neuron connections, the blue curve shows results from training with SCFF, the green curve shows Backprop results

After the first stage of unsupervised training, a linear classifier is trained on the hidden states from the final time step in both directions, as shown in the bottom of the Fig. 6a. The blue, orange and green curves in Fig. 6b depict the test accuracy of the linear output classifier with hidden connections trained using SCFF, with random (untrained) hidden connections, and with Backpropagation methods, respectively. SCFF achieves a test accuracy of 90.3% when trained with a one-layer Bi-RNN containing 500 hidden neurons in each direction (refer to Appendix E for further architectural details). It is below the performance of BackPropagation Though Time, reaching 96% accuracy on this small task, but well above the model with untrained (random) hidden connections which plateaus at 80.7%.

This result constitutes the first successful application of the FF approach to sequential data in an unsupervised manner. Unlike the BPTT method for training RNNs, SCFF avoids the issues of vanishing and exploding gradients, as the gradients at each

Table 1: Comparisons of the learning capabilities of different local learning methods and their test accuracy [%] on CIFAR-10 and STL-10 dataset.

Method	(Self)Unsupervised ¹	Local	Sequential ²	CIFAR-10	STL-10
SimCLR (Chen et. al. 2020 [49])	✓	✗	✓	94.0	89.7
PNN-SSL (Laydevant et. al. 2023 [62])	✓	✗	✗	77.0	-
Bio-SSL (Tang et. al. 2022 [63])	✓	✓	✗	72.7	68.8
CLAPP (Illing et. al. 2021 [64])	✓	✓	✗	-	73.6
SigProp (Kohan et. al. 2023 [5])	✗	✓	✗	91.6	-
EqProp (Laborieux et. al. 2021 [65])	✗	✓	✗	88.6	-
DualProp (Høier et. al. 2023 [66])	✗	✓	✗	92.3	-
FF (Hinton et. al. 2023 [19])	✓	✓	✗	59.0	-
FF (Papachristodoulou et. al. 2024 [33])	✗	✓	✗	78.1	-
FF (Wu et. al. 2024 [44])	✗	✓	✗	84.7	-
PEPITA (Srinivasan et. al. 2023 [8])	✗	✓	✗	53.8	-
Act. Learning (Zhou et. al. 2022 [7])	✓	✓	✗	58.7	-
HardHebb (Miconi et. al. 2021 [11])	✓	✓	✗	64.8	-
HardHebb (Lagani et. al. 2022 [12])	✓	✓	✗	64.6	-
Hebb-CHU (Krotov et. al. 2019 [13])	✓	✓	✗	50.8	-
Hebb-PNorm (Grinberg et. al. 2019 [67])	✓	✓	✗	72.2	-
SoftHebb (Journé et. al. 2022 [9])	✓	✓	✗	80.3	76.2
SCFF (ours)	✓	✓	✓	80.8	77.3

¹Self-supervised or unsupervised

²Can handle sequential data or not

time step are calculated independently. This eliminates the dependency between time steps, providing a more stable training process.

It is also interesting to note that the network with untrained hidden and input connections is akin to Reservoir Computing, a method that is often used to leverage physical systems on sequential data for neuromorphic applications [60]. SCFF provides a way to train these input and hidden layer connections in a simple, hardware-compatible way, and opens the path to a considerable gain of accuracy. This achievement opens the door for its extension to more complex tasks involving temporal sequences and its potential use in neuromorphic computing domains, such as dynamic vision sensors [61].

4 Discussion

4.1 Comparison to the original FF algorithm

In addressing the limitations of the original FF algorithm, our method introduces several key improvements. Firstly, we have developed an approach for generating negative examples that can be applied to any database. This approach is also biologically plausible, since it operates by aggregating two similar or different images at the input, very much like our eyes do. This innovation directly addresses the criticisms highlighted in [8], which pointed out the biological implausibility of the negative examples used in the original FF algorithm.

Furthermore, we have expanded the applicability of FF to complex unsupervised tasks beyond the MNIST dataset. The SCFF method achieves state-of-the-art (SOTA) accuracy for local methods on challenging datasets such as CIFAR-10 and STL-10,

largely outperforming the original FF algorithm (see Table 1). This is a significant advancement, as it demonstrates that our method performs comparably to other local and forward-only algorithms in complex visual tasks, thereby broadening the scope and utility of FF to unlabeled data processing.

Additionally, we have extended the capabilities of FF to include sequential task solving. This extension is crucial for applications in time-series analysis and other domains where data is inherently sequential. By incorporating these improvements, our SCFF method not only overcomes the original limitations of FF but also sets a new benchmark for unsupervised learning algorithms in terms of versatility and performance.

4.2 Comparison to SOTA self-supervised learning (SSL)

Our SCFF method draws significant inspiration from self-supervised contrastive learning techniques [49, 68]. While the accuracy of SCFF may be lower compared to these methods, primarily due to its layer-wise learning in a purely local manner, it offers unique advantages. Unlike global self-supervised methods, SCFF operates without requiring auxiliary heads (multi-layer nonlinear projector) or complex regularization techniques, which simplifies its implementation and makes it more suitable for neuromorphic computing applications.

Recent developments in local versions of contrastive self-supervised learning have shown promising results [62, 63]. For instance, Laydevant et al. [62] empirically demonstrated that layer-wise SSL objectives can be optimized rather than a single global one, achieving performance comparable to global optimization on datasets such as MNIST and CIFAR-10 (see Table 1). However, the layer-wise training methods involving multi-layer MLP as projector heads might offer better performance in certain tasks, but at the cost of increased computational complexity. Illing et al. [64] have shown that local plasticity rules, when applied through the CLAPP model, can successfully build deep hierarchical representations without the need for backpropagation. However, this method introduces additional processing along the time axis, which may add complexity when dealing with data that lacks temporal dynamics.

4.3 Comparison to other forward-only methods including non-Hebbian and Hebbian based

Recently, other purely forward learning techniques have been developed, driven by their potential for biologically plausible and neuromorphic computing applications [7, 8]. Similar to Forward-Forward (FF), Pepita [8] processes data samples in two forward passes. The first pass is identical to FF, while the input of the second pass is modulated by incorporating information about the error from the first forward pass through top-down feedback. Activation Learning [7] builds on Hebb’s well-known proposal, discovering unsupervised features through local competitions among neurons. However, these methods do not yet scale to more complex tasks, limiting their potential applications.

Recent advances in Hebbian deep learning have also shown remarkable progress [9, 11, 12, 69]. These methods are purely local in space and can be applied purely

locally in time, offering a biologically plausible approach to learning. Miconi [11] demonstrated that Hebbian learning in hierarchical convolutional neural networks can be implemented with modern deep learning frameworks by using specific losses whose gradients produce the desired Hebbian updates. However, adding layers has not resulted in significant performance improvements on standard benchmarks [11, 12] (see Table 1). Journe et al. [9] proposed using a simple softmax to implement a soft Winner-Takes-All (WTA) and derived a Hebbian-like plasticity rule (SoftHebb). With techniques like triangle activation and adjustable rectified polynomial units, SoftHebb achieves increased efficiency and biological compatibility, enhancing accuracy compared to state-of-the-art biologically plausible learning methods.

Our SCFF method brings the FF approach to accuracy levels comparable to SoftHebb, effectively bridging the gap between these learning paradigms. A key advantage of Hebbian learning is its ability to learn without contrast, much like non-contrastive self-supervised learning techniques, operating purely in an unsupervised manner. Conversely, FF is flexible regarding labels, akin to contrastive self-supervised learning techniques, supporting both unsupervised learning as we demonstrate here with SCFF and supervised learning. This versatility allows FF to be applied across a broader range of tasks and datasets, enhancing its applicability and effectiveness in diverse scenarios.

4.4 Comparison to energy-based learning methods

Energy-based learning methods, such as Equilibrium Propagation (EP), Dual Propagation (DP) and Latent Equilibrium (LE) [66, 70, 71], also offer locality in space and time. These methods have a significant advantage over SCFF due to their strong mathematical foundations, closely approximating gradients from BP and backpropagation through time (BPTT). This theoretical rigor allows them to be applied to a wide range of physical systems, making them particularly appealing for neuromorphic computing applications. EP, for instance, can operate in an unsupervised manner, while recent advancements in Generalized Latent Equilibrium (GLE) [72] have extended these models to handle sequential data effectively.

However, the implementation of energy-based methods poses certain challenges. Specifically, the backward pass in these methods requires either bidirectional neural networks or dedicated backward circuits [73, 74]. These requirements can be complex to design and build in a manner that is both energy-efficient and compact. In contrast, the simplicity and versatility of SCFF in supporting both supervised and unsupervised learning, without the need for complex backward circuitry, make it a practical alternative for many applications [3]. This balance of accuracy, ease of implementation, and versatility underscores the potential of SCFF in advancing neuromorphic computing and biologically inspired learning systems.

5 Conclusion

In conclusion, the Forward-Forward (FF) algorithm has sparked significant advancements in both biologically-inspired deep learning and hardware-efficient computation. However, its original form faced challenges in handling complex datasets and time-varying sequential data. Our method, Self Contrastive Forward-Forward (SCFF),

addresses these limitations by integrating contrastive self-supervised learning principles directly at the input level, enabling the generation of positive and negative examples through a simple concatenation of input data. SCFF not only surpasses existing unsupervised learning algorithms in accuracy on datasets like MNIST, CIFAR-10, and STL-10 but also successfully extends the FF approach to sequential data, demonstrating its applicability to a broader range of tasks. These developments pave the way for more robust and versatile applications of FF in both neuromorphic computing and beyond, opening new avenues for research and practical implementations in the field.

6 Methods

SCFF learns representations by maximizing agreement (increasing activations/-goodness) between concatenated pairs of identical data examples while minimizing agreement (reducing activations/goodness) between concatenated pairs of different data examples using a cross-entropy-like loss function at each layer. The network is trained layer by layer, with each layer’s weights being frozen before moving on to the next. Unlike the original FF framework, this approach incorporates several key components that contribute to achieving high accuracy across various tasks.

Normalization and Standardization

For vision tasks, the data is typically normalized by subtracting the mean and dividing by the standard deviation for each channel. These mean and standard deviation values are computed across the entire training dataset, separately for each of the three color channels. This dataset-wide normalization centers the data, ensuring that each channel has a mean of 0 and is on a comparable scale.

In addition to dataset-wide normalization, we also applied per-image standardization, which plays an important role in unsupervised feature learning [75]. Standardizing the images involves scaling the pixel values of each image such that the resultant pixel values of the image have a mean of 0 and a standard deviation of 1. This is done before each layer during processing [11, 47], ensuring that each sample is centered, which improves learning stability and helps the network handle varying illumination or contrast between images.

Concatenation

The positive and negative examples (e.g. $\mathbf{x}_{i,\text{pos}}^{(0)}$ and $\mathbf{x}_{j,\text{neg}}^{(0)}$) are generated by concatenating two identical images for the positive examples and two different images for the negative examples. After being processed by the first layer, the output vectors $\mathbf{y}_{i,\text{pos}}^{(0)}$ and $\mathbf{y}_{j,\text{neg}}^{(0)}$ are obtained. There are two approaches for generating the inputs to the next layer. The first approach is to directly use the first layer’s output of the positive example $\mathbf{y}_{i,\text{pos}}^{(0)}$ as the positive input $\mathbf{x}_{i,\text{pos}}^{(1)}$, and the first layer output of the negative example $\mathbf{y}_{j,\text{neg}}^{(0)}$ as the negative input $\mathbf{x}_{j,\text{neg}}^{(1)}$ for the next layer (refer to the highlighted blue section in Algorithm 1 in Appendix C). The second approach involves re-concatenating to form new positive and negative inputs for the next layer. This is done by treating the first layer’s positive outputs as a new dataset and recreating

the corresponding positive and negative examples, similar to how the original dataset was processed to generate the initial positive and negative examples (refer to the highlighted blue section in Algorithm 2 in Appendix C).

Appendix C details the workflows of Algorithm 1 and Algorithm 2, focusing on their different approaches to generating positive and negative examples after the first layer. In practice, Algorithm 1 tends to be more effective for training the lower layers immediately following the first layer, while Algorithm 2 shows better performance in training deeper layers. Specifically, for the CIFAR-10 dataset, Algorithm 1 is utilized to train the second layer, while Algorithm 2 is applied to train the third layer. Similarly, for the STL-10 dataset, Algorithm 1 is employed for training the second and third layers, and Algorithm 2 is used for the fourth layer.

Triangle method of transmitting the information

“Triangle” method was firstly introduced by Coates et al. [47] to compute the activations of the learned features by K-means clustering. This method was later found to be effective in other Hebbian-based algorithms [9, 11] for transmitting the information from one layer to the next. The method involves subtracting the mean activation (computed across all channels at a given position) from each channel, and then rectifying any negative values to zero before the pooling layer. This approach to feature mapping can be viewed as a simple form of “competition” between features while also promoting sparsity.

Importantly, the “Triangle” activation only determines the responses passed to the next layer; it does not influence the plasticity. The output used for plasticity at each position is given by $\mathbf{y}_{i,\text{pos}}^{(l)} = f^{(l)}(\mathbf{x}_{i,\text{pos}})$ and $\mathbf{y}_{i,\text{neg}}^{(l)} = f^{(l)}(\mathbf{x}_{j,\text{neg}})$, where $f^{(l)}$ refers to the convolutional operations followed by ReLU activation at layer l .

Penalty term

Training with the FF loss can lead to excessively high output activations for positive examples, which significantly drives positive gradients and encourages unchecked growth in their activation. To mitigate this, we introduce a small penalty term—the Frobenius Norm of the Goodness vector—into the training loss function. For outputs from a CNN layer, the goodness vector $G_{i,h,w,\text{pos}}^{(l)}$ is a two-dimensional matrix where each element represents the goodness calculated over the channel outputs processed by all filters under the same receptive field. In the case of Bi-RNN outputs, the goodness vector $G_{i,t,\text{pos}}^{(l)}$ is a one-dimensional matrix, with each element representing the goodness at each time step. When a large goodness value is computed for a positive example, it generates a negative gradient that reduces the activation, thereby preventing excessive growth. The impact of this penalty term on training performance is further analyzed in Appendix F.

Additional pooling operation to retrieve the features

To assess the performance of the intermediate layers in image classification tasks, we apply an additional pooling operation (average or max pooling) to the output of the

pooling layer. This reduces the dimensionality of the features and helps in selecting relevant neuron activities. This approach is inspired by the "four quadrant" method used in previous work [11, 47], where local regions extracted from the convolutional layer are divided into four equal-sized quadrants, and the sum of neuron activations in each quadrant is computed for downstream linear classification tasks.

Appendix D provides detailed information on the specific architecture of this additional pooling layer for various tasks.

Data availability. The datasets used during the current study, i.e., IRIS [51], MNIST [45], CIFAR-10 [46], STL-10 [47] and FSDD (Free Spoken Digit Dataset) [52], are available online.

Code availability. The code to reproduce the results will be made available upon publication.

Declarations

Acknowledgments. This work was supported by the European Research Council advanced grant GrenaDyn (reference: 101020684). The text of the article was partially edited by a large language model (OpenAI ChatGPT). The authors would like to thank D. Querlioz for discussion and invaluable feedback.

Author contributions statement. X.C. and J.G. devised the study. X.C. performed all the simulations and experiments. X.C., J.G, D. L and J. L actively discussed the results at every stage of the study. X.C and J.G. wrote the initial version of the manuscript. All authors reviewed the manuscript.

Competing interests. The authors declare no competing interests.

References

- [1] Hebb, D.O.: The Organization of Behavior: A Neuropsychological Theory, Reprint edition edn. Psychology Press, New York, NY (2005)
- [2] Richards, B.A., Lillicrap, T.P., Beaudoin, P., Bengio, Y., Bogacz, R., Christensen, A., Clopath, C., Costa, R.P., Berker, A., Ganguli, S., *et al.*: A deep learning framework for neuroscience. *Nature neuroscience* **22**(11), 1761–1770 (2019)
- [3] Momeni, A., Rahmani, B., Scellier, B., Wright, L.G., McMahon, P.L., Wanjura, C.C., Li, Y., Skalli, A., Berloff, N.G., Onodera, T., Oguz, I., Morichetti, F., Hougne, P., Gallo, M.L., Sebastian, A., Mirhoseini, A., Zhang, C., Marković, D., Brunner, D., Moser, C., Gigan, S., Marquardt, F., Ozcan, A., Grollier, J., Liu, A.J., Psaltis, D., Alù, A., Fleury, R.: Training of Physical Neural Networks (2024). <https://arxiv.org/abs/2406.03372>
- [4] Marković, D., Mizrahi, A., Querlioz, D., Grollier, J.: Physics for neuromorphic computing. *Nature Reviews Physics* **2**(9), 499–510 (2020)

- [5] Kohan, A., Rietman, E.A., Siegelmann, H.T.: Signal propagation: The framework for learning and inference in a forward pass. *IEEE Transactions on Neural Networks and Learning Systems* (2023)
- [6] Frenkel, C., Lefebvre, M., Bol, D.: Learning without feedback: Fixed random learning signals allow for feedforward training of deep neural networks. *Frontiers in neuroscience* **15**, 629892 (2021)
- [7] Zhou, H.: Activation learning by local competitions. *arXiv preprint arXiv:2209.13400* (2022)
- [8] Srinivasan, R.F., Mignacco, F., Sorbaro, M., Refinetti, M., Cooper, A., Kreiman, G., Dellaferrera, G.: Forward learning with top-down feedback: Empirical and analytical characterization. *arXiv preprint arXiv:2302.05440* (2023)
- [9] Journé, A., Rodriguez, H.G., Guo, Q., Moraitis, T.: Hebbian deep learning without feedback. *arXiv preprint arXiv:2209.11883* (2022)
- [10] Stuhr, B., Brauer, J.: Csnns: Unsupervised, backpropagation-free convolutional neural networks for representation learning. In: 2019 18th IEEE International Conference On Machine Learning And Applications (ICMLA), pp. 1613–1620 (2019). IEEE
- [11] Miconi, T.: Hebbian learning with gradients: Hebbian convolutional neural networks with modern deep learning frameworks. *arXiv preprint arXiv:2107.01729* (2021)
- [12] Lagani, G., Falchi, F., Gennaro, C., Amato, G.: Comparing the performance of hebbian against backpropagation learning using convolutional neural networks. *Neural Computing and Applications* **34**(8), 6503–6519 (2022)
- [13] Krotov, D., Hopfield, J.J.: Unsupervised learning by competing hidden units. *Proceedings of the National Academy of Sciences* **116**(16), 7723–7731 (2019)
- [14] Lorberbom, G., Gat, I., Adi, Y., Schwing, A., Hazan, T.: Layer collaboration in the forward-forward algorithm. In: *Proceedings of the AAAI Conference on Artificial Intelligence*, vol. 38, pp. 14141–14148 (2024)
- [15] Deng, Q., Jin, G., Noh, Y., Yu, S., Lee, D.: Dff: Distributed forward-forward algorithm for large-scale model in low-performance devices. In: 2023 IEEE 6th International Conference on Pattern Recognition and Artificial Intelligence (PRAI), pp. 1218–1223 (2023). IEEE
- [16] Aktemur, E., Zorlutuna, E., Bilgili, K., Bok, T.E., Yanikoglu, B., Mutluergil, S.O.: Going forward-forward in distributed deep learning. *arXiv preprint arXiv:2404.08573* (2024)

- [17] Malladi, S., Gao, T., Nichani, E., Damian, A., Lee, J.D., Chen, D., Arora, S.: Fine-tuning language models with just forward passes. *Advances in Neural Information Processing Systems* **36**, 53038–53075 (2023)
- [18] Xu, M., Wu, Y., Cai, D., Li, X., Wang, S.: Federated fine-tuning of billion-sized language models across mobile devices. *arXiv preprint arXiv:2308.13894* (2023)
- [19] Hinton, G.: The forward-forward algorithm: Some preliminary investigations. *arXiv preprint arXiv:2212.13345* (2022)
- [20] Williams, E., Bredenberg, C., Lajoie, G.: Flexible phase dynamics for bioplausible contrastive learning. In: *International Conference on Machine Learning*, pp. 37042–37065 (2023). PMLR
- [21] Lv, C., Gu, Y., Guo, Z., Xu, Z., Wu, Y., Zhang, F., Shi, T., Wang, Z., Yin, R., Shang, Y., et al.: Towards biologically plausible computing: A comprehensive comparison. *arXiv preprint arXiv:2406.16062* (2024)
- [22] Ororbia, A., Mali, A., Kohan, A., Millidge, B., Salvatori, T.: A review of neuroscience-inspired machine learning. *arXiv preprint arXiv:2403.18929* (2024)
- [23] Farinha, M.T., Ortner, T., Dellaferrera, G., Grewe, B., Pantazi, A.: Efficient biologically plausible adversarial training. *arXiv preprint arXiv:2309.17348* (2023)
- [24] Guan, J., Verch, S.E., Voelcker, C.A., Jackson, E.C., Papernot, N., Cunningham, W.A.: Local-forward: Towards biological plausibility in deep reinforcement learning
- [25] Momeni, A., Rahmani, B., Malléjac, M., Hougne, P., Fleury, R.: PhyFF: Physical forward forward algorithm for in-hardware training and inference. In: *Machine Learning with New Compute Paradigms* (2023). <https://openreview.net/forum?id=aqsFLVg0tY>
- [26] Zhu, H., Chen, Y., Hu, G., Yu, S.: Contrastive learning via local activity. *Electronics* **12**(1), 147 (2022)
- [27] Flügel, K., Coquelin, D., Weiel, M., Debus, C., Streit, A., Götz, M.: Feed-forward optimization with delayed feedback for neural networks. *arXiv preprint arXiv:2304.13372* (2023)
- [28] Ororbia, A., Mali, A.: The predictive forward-forward algorithm. *arXiv preprint arXiv:2301.01452* (2023)
- [29] Giampaolo, F., Izzo, S., Prezioso, E., Piccialli, F.: Investigating random variations of the forward-forward algorithm for training neural networks. In: *2023 International Joint Conference on Neural Networks (IJCNN)*, pp. 1–7 (2023). IEEE

- [30] Zhao, G., Wang, T., Li, Y., Jin, Y., Lang, C., Ling, H.: The cascaded forward algorithm for neural network training. arXiv preprint arXiv:2303.09728 (2023)
- [31] Tosato, N., Basile, L., Ballarin, E., De Alteriis, G., Cazzaniga, A., Ansuini, A.: Emergent representations in networks trained with the forward-forward algorithm. arXiv preprint arXiv:2305.18353 (2023)
- [32] Lee, H.-C., Song, J.: Symba: Symmetric backpropagation-free contrastive learning with forward-forward algorithm for optimizing convergence. arXiv preprint arXiv:2303.08418 (2023)
- [33] Papachristodoulou, A., Kyrkou, C., Timotheou, S., Theocharides, T.: Convolutional channel-wise competitive learning for the forward-forward algorithm. In: Proceedings of the AAAI Conference on Artificial Intelligence, vol. 38, pp. 14536–14544 (2024)
- [34] Reyes-Angulo, A.A., Paheding, S.: Forward-forward algorithm for hyperspectral image classification. In: Proceedings of the IEEE/CVF Conference on Computer Vision and Pattern Recognition, pp. 3153–3161 (2024)
- [35] Scodellaro, R., Kulkarni, A., Alves, F., Schröter, M.: Training convolutional neural networks with the forward-forward algorithm. arXiv preprint arXiv:2312.14924 (2023)
- [36] Yang, Y.: A theory for the sparsity emerged in the forward forward algorithm. arXiv preprint arXiv:2311.05667 (2023)
- [37] Gananath, R.: Improved forward-forward contrastive learning. arXiv preprint arXiv:2405.03432 (2024)
- [38] Hwang, T., Seo, H., Jung, S.: Employing layerwised unsupervised learning to lessen data and loss requirements in forward-forward algorithms. arXiv preprint arXiv:2404.14664 (2024)
- [39] Kam, F.d.: Memory consolidation by deep-q forward-forward learning in games. PhD thesis, University of Groningen, Faculty of Science and Engineering (2024)
- [40] De Vita, F., Nawaiseh, R.M., Bruneo, D., Tomaselli, V., Lattuada, M., Falchetto, M.: μ -ff: On-device forward-forward training algorithm for microcontrollers. In: 2023 IEEE International Conference on Smart Computing (SMARTCOMP), pp. 49–56 (2023). IEEE
- [41] Park, S.-H., Ko, J., Lee, I.-S., Koo, R.-H., Kim, J.-H., Yang, Y., Kwon, D., Kim, J.-J., Lee, J.-H.: On-chip learning in vertical nand flash memory using forward-forward algorithm. IEEE Transactions on Electron Devices (2024)
- [42] Momeni, A., Rahmani, B., Malléjac, M., Del Hougne, P., Fleury, R.:

- Backpropagation-free training of deep physical neural networks. *Science* **382**(6676), 1297–1303 (2023)
- [43] Oguz, I., Ke, J., Weng, Q., Yang, F., Yildirim, M., Dinc, N.U., Hsieh, J.-L., Moser, C., Psaltis, D.: Forward-forward training of an optical neural network. *Optics Letters* **48**(20), 5249–5252 (2023)
- [44] Wu, Y., Xu, S., Wu, J., Deng, L., Xu, M., Wen, Q., Li, G.: Distance-forward learning: Enhancing the forward-forward algorithm towards high-performance on-chip learning. *arXiv preprint arXiv:2408.14925* (2024)
- [45] Deng, L.: The mnist database of handwritten digit images for machine learning research. *IEEE Signal Processing Magazine* **29**(6), 141–142 (2012)
- [46] Krizhevsky, A., Nair, V., Hinton, G.: Cifar-10 (canadian institute for advanced research)
- [47] Coates, A., Ng, A., Lee, H.: An analysis of single-layer networks in unsupervised feature learning. In: *Proceedings of the Fourteenth International Conference on Artificial Intelligence and Statistics*, pp. 215–223 (2011). *JMLR Workshop and Conference Proceedings*
- [48] Gutmann, M., Hyvärinen, A.: Noise-contrastive estimation: A new estimation principle for unnormalized statistical models. In: *Proceedings of the Thirteenth International Conference on Artificial Intelligence and Statistics*, pp. 297–304 (2010). *JMLR Workshop and Conference Proceedings*
- [49] Chen, T., Kornblith, S., Norouzi, M., Hinton, G.: A simple framework for contrastive learning of visual representations. In: *International Conference on Machine Learning*, pp. 1597–1607 (2020). *PMLR*
- [50] Lee, K., Yun, S., Lee, K., Lee, H., Li, B., Shin, J.: Robust inference via generative classifiers for handling noisy labels. In: *International Conference on Machine Learning*, pp. 3763–3772 (2019). *PMLR*
- [51] Fisher, R.A.: Iris. *UCI Machine Learning Repository*. DOI: <https://doi.org/10.24432/C56C76> (1988)
- [52] Jackson, Z., Souza, C., Flaks, J., Pan, Y., Nicolas, H., Thite, A.: Jakobovski/free-spoken-digit-dataset: v1. 0.8. *Zenodo* (2018)
- [53] Alain, G.: Understanding intermediate layers using linear classifier probes. *arXiv preprint arXiv:1610.01644* (2016)
- [54] Lafabregue, B., Weber, J., Gañçarski, P., Forestier, G.: Grad centroid activation mapping for convolutional neural networks. In: *2021 IEEE 33rd International Conference on Tools with Artificial Intelligence (ICTAI)*, pp. 184–191 (2021). *IEEE*

- [55] Van-Horenbeke, F.A., Peer, A.: Nilrnn: a neocortex-inspired locally recurrent neural network for unsupervised feature learning in sequential data. *Cognitive Computation* **15**(5), 1549–1565 (2023)
- [56] Limbacher, T., Özdenizci, O., Legenstein, R.: Memory-enriched computation and learning in spiking neural networks through hebbian plasticity. arXiv preprint arXiv:2205.11276 (2022)
- [57] Gokul, V., Dubnov, S.: Poscuda: Position based convolution for unlearnable audio datasets. arXiv preprint arXiv:2401.02135 (2024)
- [58] Tiwari, V.: Mfcc and its applications in speaker recognition. *International journal on emerging technologies* **1**(1), 19–22 (2010)
- [59] Schuster, M., Paliwal, K.K.: Bidirectional recurrent neural networks. *IEEE transactions on Signal Processing* **45**(11), 2673–2681 (1997)
- [60] Abreu Araujo, F., Riou, M., Torrejon, J., Tsunegi, S., Querlioz, D., Yakushiji, K., Fukushima, A., Kubota, H., Yuasa, S., Stiles, M.D., *et al.*: Role of non-linear data processing on speech recognition task in the framework of reservoir computing. *Scientific reports* **10**(1), 328 (2020)
- [61] He, W., Wu, Y., Deng, L., Li, G., Wang, H., Tian, Y., Ding, W., Wang, W., Xie, Y.: Comparing snns and rnns on neuromorphic vision datasets: Similarities and differences. *Neural Networks* **132**, 108–120 (2020)
- [62] Laydevant, J., McMahon, P., Venturelli, D., Lott, P.A.: The benefits of self-supervised learning for training physical neural networks. In: *Machine Learning with New Compute Paradigms* (2023)
- [63] Tang, M., Yang, Y., Amit, Y.: Biologically plausible training mechanisms for self-supervised learning in deep networks. *Frontiers in computational neuroscience* **16**, 789253 (2022)
- [64] Illing, B., Ventura, J., Bellec, G., Gerstner, W.: Local plasticity rules can learn deep representations using self-supervised contrastive predictions. *Advances in neural information processing systems* **34**, 30365–30379 (2021)
- [65] Laborieux, A., Ernoult, M., Scellier, B., Bengio, Y., Grollier, J., Querlioz, D.: Scaling equilibrium propagation to deep convnets by drastically reducing its gradient estimator bias. *Frontiers in neuroscience* **15**, 633674 (2021)
- [66] Høier, R., Staudt, D., Zach, C.: Dual propagation: Accelerating contrastive hebbian learning with dyadic neurons. In: *International Conference on Machine Learning*, pp. 13141–13156 (2023). PMLR
- [67] Grinberg, L., Hopfield, J., Krotov, D.: Local unsupervised learning for image

- analysis. arXiv preprint arXiv:1908.08993 (2019)
- [68] He, K., Fan, H., Wu, Y., Xie, S., Girshick, R.: Momentum contrast for unsupervised visual representation learning. In: Proceedings of the IEEE/CVF Conference on Computer Vision and Pattern Recognition, pp. 9729–9738 (2020)
 - [69] Lagani, G., Gennaro, C., Fassold, H., Amato, G.: Fasthebb: Scaling hebbian training of deep neural networks to imagenet level. In: International Conference on Similarity Search and Applications, pp. 251–264 (2022). Springer
 - [70] Scellier, B., Bengio, Y.: Equilibrium propagation: Bridging the gap between energy-based models and backpropagation. *Frontiers in computational neuroscience* **11**, 24 (2017)
 - [71] Haider, P., Ellenberger, B., Kriener, L., Jordan, J., Senn, W., Petrovici, M.A.: Latent equilibrium: A unified learning theory for arbitrarily fast computation with arbitrarily slow neurons. *Advances in neural information processing systems* **34**, 17839–17851 (2021)
 - [72] Ellenberger, B., Haider, P., Jordan, J., Max, K., Jaras, I., Kriener, L., Benitez, F., Petrovici, M.A.: Backpropagation through space, time, and the brain. arXiv preprint arXiv:2403.16933 (2024)
 - [73] Kendall, J., Pantone, R., Manickavasagam, K., Bengio, Y., Scellier, B.: Training end-to-end analog neural networks with equilibrium propagation. arXiv preprint arXiv:2006.01981 (2020)
 - [74] Yi, S.-i., Kendall, J.D., Williams, R.S., Kumar, S.: Activity-difference training of deep neural networks using memristor crossbars. *Nature Electronics* **6**(1), 45–51 (2023)
 - [75] Huang, L., Qin, J., Zhou, Y., Zhu, F., Liu, L., Shao, L.: Normalization techniques in training dnns: Methodology, analysis and application. *IEEE transactions on pattern analysis and machine intelligence* **45**(8), 10173–10196 (2023)

Appendix A On the convergence of W_1 and W_2

The loss function of the SCFF method for one pair of positive input and negative input examples in the first layer (the layer index is neglected here) is defined as

$$\ell_{i,j} = \log(1 + \exp(\Theta - \|\mathbf{y}_{i,\text{pos}}\|^2)) + \log(1 + \exp(\|\mathbf{y}_{j,\text{neg}}\|^2 - \Theta)) \quad (\text{A.1})$$

where $\|\mathbf{y}_{i,\text{pos}}\|^2$ and $\|\mathbf{y}_{j,\text{neg}}\|^2$ represent sum of the square of neuron activations respectively. The same procedure applies if mean activations are used instead. For simplicity, both threshold values Θ_{pos} and Θ_{neg} are assumed to be equal, i.e., $\Theta = \Theta_{\text{pos}} = \Theta_{\text{neg}}$. However, the same conclusion holds even if different thresholds are assumed for the positive and negative examples. $\mathbf{y}_{i,\text{pos}}$ and $\mathbf{y}_{j,\text{neg}}$ are calculated as

$$\mathbf{y}_{i,\text{pos}} = f(W_1 \mathbf{x}_k + W_2 \mathbf{x}_k) \quad (\text{A.2})$$

$$\mathbf{y}_{j,\text{neg}} = f(W_1 \mathbf{x}_k + W_2 \mathbf{x}_n) \quad (\text{A.3})$$

where \mathbf{x}_k is a randomly selected example, and \mathbf{x}_n is assumed to come from a different class of \mathbf{x}_k . f is the ReLU activation function.

The derivative of $\ell_{i,j}$ with respect to W_1 and W_2 are respectively

$$\frac{\partial \ell_{i,j}}{\partial W_1} = \frac{-\exp(\Theta - \|\mathbf{y}_{i,\text{pos}}\|^2)}{(1 + \exp(\Theta - \|\mathbf{y}_{i,\text{pos}}\|^2))} \frac{\partial \|\mathbf{y}_{i,\text{pos}}\|^2}{\partial W_1} + \frac{\exp(\|\mathbf{y}_{j,\text{neg}}\|^2 - \Theta)}{(1 + \exp(\|\mathbf{y}_{j,\text{neg}}\|^2 - \Theta))} \frac{\partial \|\mathbf{y}_{j,\text{neg}}\|^2}{\partial W_1} \quad (\text{A.4})$$

$$\frac{\partial \ell_{i,j}}{\partial W_2} = \frac{-\exp(\Theta - \|\mathbf{y}_{i,\text{pos}}\|^2)}{(1 + \exp(\Theta - \|\mathbf{y}_{i,\text{pos}}\|^2))} \frac{\partial \|\mathbf{y}_{i,\text{pos}}\|^2}{\partial W_2} + \frac{\exp(\|\mathbf{y}_{j,\text{neg}}\|^2 - \Theta)}{(1 + \exp(\|\mathbf{y}_{j,\text{neg}}\|^2 - \Theta))} \frac{\partial \|\mathbf{y}_{j,\text{neg}}\|^2}{\partial W_2} \quad (\text{A.5})$$

As we consider that f is a ReLU activation function such that $\frac{\partial \|\mathbf{y}_{i,\text{pos}}\|^2}{\partial W_1} = \frac{\partial \mathbf{y}_{i,\text{pos}}^T \mathbf{y}_{i,\text{pos}}}{\partial W_1} = 2 \cdot \text{diag}(f'_{\mathbf{y}_{i,\text{pos}}}) \cdot \mathbf{y}_{i,\text{pos}} \cdot \mathbf{x}_k^T$ where $\text{diag}(f'_{\mathbf{y}_{i,\text{pos}}})$ is a diagonal matrix with elements being the derivatives of ReLU applied element-wise to $\mathbf{y}_{i,\text{pos}}$. Therefore, we are able to obtain

$$\begin{aligned} \frac{\partial \ell_{i,j}}{\partial W_1} &= \frac{-\exp(\Theta - \|\mathbf{y}_{i,\text{pos}}\|^2)}{(1 + \exp(\Theta - \|\mathbf{y}_{i,\text{pos}}\|^2))} (2 \cdot \text{diag}(f'_{\mathbf{y}_{i,\text{pos}}}) \cdot \mathbf{y}_{i,\text{pos}} \cdot \mathbf{x}_k^T) + \\ &\quad \frac{\exp(\|\mathbf{y}_{j,\text{neg}}\|^2 - \Theta)}{(1 + \exp(\|\mathbf{y}_{j,\text{neg}}\|^2 - \Theta))} (2 \cdot \text{diag}(f'_{\mathbf{y}_{j,\text{neg}}}) \cdot \mathbf{y}_{j,\text{neg}} \cdot \mathbf{x}_k^T) \quad (\text{A.6}) \\ \frac{\partial \ell_{i,j}}{\partial W_2} &= \frac{-\exp(\Theta - \|\mathbf{y}_{i,\text{pos}}\|^2)}{(1 + \exp(\Theta - \|\mathbf{y}_{i,\text{pos}}\|^2))} (2 \cdot \text{diag}(f'_{\mathbf{y}_{i,\text{pos}}}) \cdot \mathbf{y}_{i,\text{pos}} \cdot \mathbf{x}_k^T) + \end{aligned}$$

$$\frac{\exp(\|\mathbf{y}_{j,\text{neg}}\|^2 - \Theta)}{(1 + \exp(\|\mathbf{y}_{j,\text{neg}}\|^2 - \Theta))} (2 \cdot \text{diag}(f'_{\mathbf{y}_{j,\text{neg}}}) \cdot \mathbf{y}_{j,\text{neg}} \cdot \mathbf{x}_n^T) \quad (\text{A.7})$$

In each update for a batch of samples, we compute the average gradient of the Loss with respect to W_1 and W_2

$$\begin{aligned} \mathbb{E}_{i,j} \left[\frac{\partial \ell_{i,j}}{\partial W_1} \right] &= \mathbb{E}_i \left[\frac{-\exp(\Theta - \|\mathbf{y}_{i,\text{pos}}\|^2)}{(1 + \exp(\Theta - \|\mathbf{y}_{i,\text{pos}}\|^2))} (2 \cdot \text{diag}(f'_{\mathbf{y}_{i,\text{pos}}}) \cdot \mathbf{y}_{i,\text{pos}} \cdot \mathbf{x}_k^T) \right] + \\ &\quad \mathbb{E}_j \left[\frac{\exp(\|\mathbf{y}_{j,\text{neg}}\|^2 - \Theta)}{(1 + \exp(\|\mathbf{y}_{j,\text{neg}}\|^2 - \Theta))} (2 \cdot \text{diag}(f'_{\mathbf{y}_{j,\text{neg}}}) \cdot \mathbf{y}_{j,\text{neg}} \cdot \mathbf{x}_k^T) \right] \end{aligned} \quad (\text{A.8})$$

$$\begin{aligned} \mathbb{E}_{i,j} \left[\frac{\partial \ell_{i,j}}{\partial W_2} \right] &= \mathbb{E}_i \left[\frac{-\exp(\Theta - \|\mathbf{y}_{i,\text{pos}}\|^2)}{(1 + \exp(\Theta - \|\mathbf{y}_{i,\text{pos}}\|^2))} (2 \cdot \text{diag}(f'_{\mathbf{y}_{i,\text{pos}}}) \cdot \mathbf{y}_{i,\text{pos}} \cdot \mathbf{x}_k^T) \right] + \\ &\quad \mathbb{E}_j \left[\frac{\exp(\|\mathbf{y}_{j,\text{neg}}\|^2 - \Theta)}{(1 + \exp(\|\mathbf{y}_{j,\text{neg}}\|^2 - \Theta))} (2 \cdot \text{diag}(f'_{\mathbf{y}_{j,\text{neg}}}) \cdot \mathbf{y}_{j,\text{neg}} \cdot \mathbf{x}_n^T) \right] \end{aligned} \quad (\text{A.9})$$

Practically, for each positive pair of $(\mathbf{x}_k, \mathbf{x}_k)$, pairs of $(\mathbf{x}_k, \mathbf{x}_n)$ and $(\mathbf{x}_n, \mathbf{x}_k)$ both work as negative samples. It is therefore natural to prove that

$$\begin{aligned} \mathbb{E}_j \frac{\exp(\|\mathbf{y}_{j,\text{neg}}\|^2 - \Theta)}{(1 + \exp(\|\mathbf{y}_{j,\text{neg}}\|^2 - \Theta))} (2 \cdot \text{diag}(f'_{\mathbf{y}_{j,\text{neg}}}) \cdot \mathbf{y}_{j,\text{neg}} \cdot \mathbf{x}_k^T) &= \\ \mathbb{E}_j \frac{\exp(\|\mathbf{y}_{j,\text{neg}}\|^2 - \Theta)}{(1 + \exp(\|\mathbf{y}_{j,\text{neg}}\|^2 - \Theta))} (2 \cdot \text{diag}(f'_{\mathbf{y}_{j,\text{neg}}}) \cdot \mathbf{y}_{j,\text{neg}} \cdot \mathbf{x}_n^T) & \end{aligned} \quad (\text{A.10})$$

Thus we have

$$\mathbb{E}_{i,j} \left[\frac{\partial L}{\partial W_1} \right] = \mathbb{E}_{i,j} \left[\frac{\partial L}{\partial W_2} \right] \quad (\text{A.11})$$

The gradient of W_1 and W_2 goes into the same direction and thus converge to each other.

Appendix B Theoretical analysis of distributions of positive and negative examples

Assuming that each class of data samples follows a multivariate Gaussian distribution, which is a commonly used assumption [S1]. Then, two examples \mathbf{x}_k and \mathbf{x}_n taken from different classes would follow:

$$\begin{aligned}\mathbf{x}_k &\sim \mathcal{N}(\boldsymbol{\mu}_1, \boldsymbol{\Sigma}_1) \\ \mathbf{x}_n &\sim \mathcal{N}(\boldsymbol{\mu}_2, \boldsymbol{\Sigma}_2)\end{aligned}$$

where $\boldsymbol{\mu}_1$ and $\boldsymbol{\mu}_2$ are the mean vectors of the two distributions, and $\boldsymbol{\Sigma}_1$ and $\boldsymbol{\Sigma}_2$ are their respective covariance matrices. Each class of distributions is assumed to be independent of each other.

Based on the previous conclusion that the input metrics W_1 and W_2 corresponding to the two concatenated images will converge to the same one and thus W_1 and W_2 is set to the same as $W = W_1 = W_2$ (the same case for all different network structures). The output becomes $\mathbf{y}_{i,\text{pos}}^{(0)} = f(2W\mathbf{x}_k)$, $\mathbf{y}_{j,\text{neg}}^{(0)} = f(W(\mathbf{x}_k + \mathbf{x}_n))$. Thus, it is clearly seen that the positive and negative examples $\mathbf{x}_{i,\text{pos}}^{(0)}$, $\mathbf{x}_{j,\text{neg}}^{(0)}$ follow (considering \mathbf{x}_k and \mathbf{x}_n is independent of each other)

$$\begin{aligned}\mathbf{x}_{i,\text{pos}}^{(0)} &\sim 2\mathbf{x}_k \sim \mathcal{N}(2\boldsymbol{\mu}_1, 2\boldsymbol{\Sigma}_1) \\ \mathbf{x}_{j,\text{neg}}^{(0)} &\sim \mathbf{x}_k + \mathbf{x}_n \sim \mathcal{N}(\boldsymbol{\mu}_1 + \boldsymbol{\mu}_2, \boldsymbol{\Sigma}_1 + \boldsymbol{\Sigma}_2)\end{aligned}$$

By further assuming that all classes share the same covariance matrix [S1], i.e., $\boldsymbol{\Sigma}_1 = \boldsymbol{\Sigma}_2 = \boldsymbol{\Sigma}$, we have

$$\begin{aligned}\mathbf{x}_{i,\text{pos}}^{(0)} &\sim \mathcal{N}(\boldsymbol{\mu}_{i,\text{p}}, \boldsymbol{\Sigma}_{i,\text{p}}) \sim \mathcal{N}(2\boldsymbol{\mu}_1, 2\boldsymbol{\Sigma}) \\ \mathbf{x}_{j,\text{neg}}^{(0)} &\sim \mathcal{N}(\boldsymbol{\mu}_{j,\text{n}}, \boldsymbol{\Sigma}_{j,\text{n}}) \sim \mathcal{N}(\boldsymbol{\mu}_1 + \boldsymbol{\mu}_2, 2\boldsymbol{\Sigma})\end{aligned}$$

It is immediately seen that the distributions of positive examples $\mathbf{x}_{i,\text{pos}}^{(0)}$ and negative examples $\mathbf{x}_{j,\text{neg}}^{(0)}$ share similar covariance properties. Besides, calculating Bhattacharyya distance (or, similarly using KL divergence), which is a measure of divergence between two probability distributions, could give more intuitive understandings of the relative positions between two different positive examples or between positive and negative examples. Denoting D_{pp} the distance between two positive distributions of $\mathbf{x}_{i,\text{pos}}^{(0)}$ and $\mathbf{x}_{j,\text{pos}}^{(0)}$, we have

$$\begin{aligned}D_{pp} &= \frac{1}{8}(\boldsymbol{\mu}_{i,\text{p}} - \boldsymbol{\mu}_{j,\text{p}})^T \left(\frac{\boldsymbol{\Sigma}_{i,\text{p}} + \boldsymbol{\Sigma}_{j,\text{p}}}{2} \right)^{-1} (\boldsymbol{\mu}_{i,\text{p}} - \boldsymbol{\mu}_{j,\text{p}}) + \frac{1}{2} \log \left(\frac{\det \left(\frac{\boldsymbol{\Sigma}_{i,\text{p}} + \boldsymbol{\Sigma}_{j,\text{p}}}{2} \right)}{\sqrt{\det \boldsymbol{\Sigma}_{i,\text{p}} \cdot \det \boldsymbol{\Sigma}_{j,\text{p}}}} \right) \\ &= \frac{1}{4}(\boldsymbol{\mu}_1 - \boldsymbol{\mu}_2)^T \boldsymbol{\Sigma}^{-1} (\boldsymbol{\mu}_1 - \boldsymbol{\mu}_2)\end{aligned}\tag{B.12}$$

Similarly, the Bhattacharya distance D_{pn} between two positive and negative distributions is calculated as

$$\begin{aligned}
D_{pn} &= \frac{1}{8}(\boldsymbol{\mu}_{i,p} - \boldsymbol{\mu}_{j,n})^T \left(\frac{\boldsymbol{\Sigma}_{i,p} + \boldsymbol{\Sigma}_{j,n}}{2} \right)^{-1} (\boldsymbol{\mu}_{i,p} - \boldsymbol{\mu}_{j,n}) + \frac{1}{2} \log \left(\frac{\det \left(\frac{\boldsymbol{\Sigma}_{i,p} + \boldsymbol{\Sigma}_{j,n}}{2} \right)}{\sqrt{\det \boldsymbol{\Sigma}_{i,p} \cdot \det \boldsymbol{\Sigma}_{j,n}}} \right) \\
&= \frac{1}{16}(\boldsymbol{\mu}_1 - \boldsymbol{\mu}_2)^T \boldsymbol{\Sigma}^{-1}(\boldsymbol{\mu}_1 - \boldsymbol{\mu}_2)
\end{aligned} \tag{B.13}$$

Thus, we find that $D_{pn} = 1/4D_{pp}$. This indicates that the negative examples are consistently positioned between two distinct clusters of positive examples within the sample space.

When positive and negative examples are projected into the feature space through a neural network, the negative examples consistently play a crucial role in enhancing the separation between the positive examples. In Fig. B.1, we demonstrate the progression of feature separation in Linear Discriminant Analysis (LDA) space across different training epochs using the Iris dataset, where the Versicolor and Virginica classes are inherently non-linearly separable. The features are first extracted via a single-layer neural network with 10 hidden neurons and subsequently mapped into the LDA space. At the initial stage (Epoch 0), there is significant overlap between the two positive classes. However, as training advances, the negative examples increasingly contribute to the improved separation of the positive classes by providing contrast that facilitates the learning of more distinct decision boundaries.

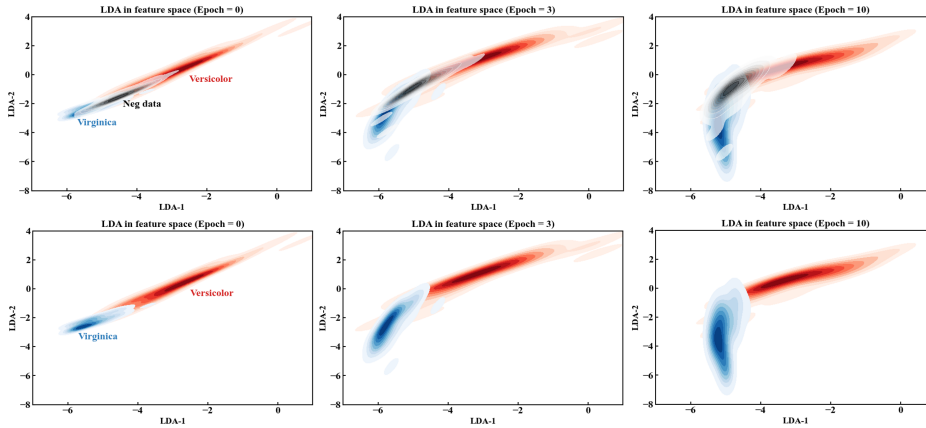


Fig. B.1: Illustration of the evolution of feature separation in Linear Discriminant Analysis (LDA) space over different training epochs. The figures depict the separation between two positive examples (Versicolor and Virginica) in the feature space at different stages of training (Epoch 0, 3, and 10). Initially, at Epoch 0, the two positive examples exhibit significant overlap. As training progresses, the negative examples contribute to improving the separation between the positive examples. The negative examples provide contrast that aids in learning better decision boundaries, ultimately leading to more effective class separation. The first row includes also the position of negative examples during the train.

Appendix C Detailed training algorithms

We present the detailed algorithms for training with convolutional layers. Algorithm 1 describes the process of training a hidden layer using positive and negative examples directly derived from the output of the previous layer’s positive and negative examples. Algorithm 2 details the training process where positive and negative examples are generated by re-concatenating the previous layer’s outputs to form new positive and negative examples. Differences between the two algorithms are highlighted in blue.

Algorithm 1 SCFF’s main learning algorithm 1

```

for each layer of structure  $f_\theta^{(l)}$ , batch size  $N$ , threshold  $\Theta_{\text{pos}}^{(l)}, \Theta_{\text{neg}}^{(l)}$  do
  for sampled minibatch  $\{\mathbf{x}_k\}_{k=1}^N$  do
    randomly select an integer  $s \in \{1, N\}$ 
    if  $l = 0$  then
      # form the positive and negative examples
       $\mathbf{x}_k = \text{std}(\mathbf{x}_k)$  # standardization
       $\mathbf{x}_{i,\text{pos}}^{(l)} = \text{cat}([\mathbf{x}_k, \mathbf{x}_k], \text{dim} = 1)$  # concatenation
       $\mathbf{x}_{j,\text{neg}}^{(l)} = \text{cat}([\mathbf{x}_k, \mathbf{x}_n], \text{dim} = 1)$  where  $n = (k + s)\%N$ 
    else
      # for  $l > 0$ 
       $\mathbf{x}_{i,\text{pos}}^{(l)} = \mathbf{y}_{i,\text{pos}}^{(l-1)}$  # previous layer output
       $\mathbf{x}_{j,\text{neg}}^{(l)} = \mathbf{y}_{j,\text{neg}}^{(l-1)}$ 
    end if
     $\mathbf{x}_{i,\text{pos}}^{(l)} = \text{std}(\mathbf{x}_{i,\text{pos}}^{(l)}); \mathbf{x}_{j,\text{neg}}^{(l)} = \text{std}(\mathbf{x}_{j,\text{neg}}^{(l)})$  # standardization
     $\mathbf{y}_{i,\text{pos}}^{(l)} = f_\theta^{(l)}(\mathbf{x}_{i,\text{pos}}^{(l)}); \mathbf{y}_{j,\text{neg}}^{(l)} = f_\theta^{(l)}(\mathbf{x}_{j,\text{neg}}^{(l)})$  # output [C, H, W]
    # calculate the goodness
     $G_{i,\text{pos}}^{(l)} = \frac{1}{C} \sum_c \mathbf{y}_{i,c,h,w,\text{pos}}^{2(l)}; G_{j,\text{neg}}^{(l)} = \frac{1}{C} \sum_c \mathbf{y}_{j,c,h,w,\text{neg}}^{2(l)}$  # output [H, W]
    #  $\mathcal{L}_{\text{SCFF}}^{(l)}$  is initialized as 0 at each layer and is accumulated for each batch
     $\mathcal{L}_{\text{SCFF}}^{(l)} = \mathcal{L}_{\text{SCFF}}^{(l)} + \ell_{i,j}$ 
    # triangle method to transmit previous layer’s information
     $\mathbf{y}_{i,\text{pos}}^{(l)} = \text{triangle}(\mathbf{y}_{i,\text{pos}}^{(l)}); \mathbf{y}_{j,\text{neg}}^{(l)} = \text{triangle}(\mathbf{y}_{j,\text{neg}}^{(l)})$ 
  end for
  Use optimizer to update network  $f_\theta^{(l)}$  to minimize  $\mathcal{L}_{\text{SCFF}}^{(l)}$ 
  # pooling operation to reduce the size of the feature maps
   $\mathbf{y}_{i,\text{pos}}^{(l)} = \text{POOL}(\mathbf{y}_{i,\text{pos}}^{(l)}); \mathbf{y}_{j,\text{neg}}^{(l)} = \text{POOL}(\mathbf{y}_{j,\text{neg}}^{(l)})$ 
end for

```

Algorithm 2 SCFF's main learning algorithm 2

```
for each layer of structure  $f_\theta^{(l)}$ , batch size  $N$ , threshold  $\Theta_{\text{pos}}^{(l)}, \Theta_{\text{neg}}^{(l)}$  do
  for sampled minibatch  $\{\mathbf{x}_k\}_{k=1}^N$  do
    randomly select an integer  $s \in \{1, N\}$ 
    if  $l = 0$  then
      # form the positive and negative examples
       $\mathbf{x}_k = \text{std}(\mathbf{x}_k)$  # standardization
       $\mathbf{x}_{i,\text{pos}}^{(l)} = \text{cat}([\mathbf{x}_k, \mathbf{x}_k], \text{dim} = 1)$  # concatenation
       $\mathbf{x}_{j,\text{neg}}^{(l)} = \text{cat}([\mathbf{x}_k, \mathbf{x}_n], \text{dim} = 1)$  where  $n = (k + s)\%N$ 
    else
      # for  $l > 0$ 
      # reconcatenation to form new positive and negative examples
       $\mathbf{x}_{i,\text{pos}}^{(l)} = \text{cat}([\text{std}(\mathbf{y}_{i,\text{pos}}^{(l-1)}), \text{std}(\mathbf{y}_{i,\text{pos}}^{(l-1)})], \text{dim} = 1)$ 
       $\mathbf{x}_{i,\text{neg}}^{(l)} = \text{cat}([\text{std}(\mathbf{y}_{j,\text{pos}}^{(l-1)}), \text{std}(\mathbf{y}_{j,\text{pos}}^{(l-1)})], \text{dim} = 1)$  where  $j = (k + s)\%N$ 
    end if
     $\mathbf{x}_{i,\text{pos}}^{(l)} = \text{std}(\mathbf{x}_{i,\text{pos}}^{(l)}); \mathbf{x}_{j,\text{neg}}^{(l)} = \text{std}(\mathbf{x}_{j,\text{neg}}^{(l)})$  # standardization
     $\mathbf{y}_{i,\text{pos}}^{(l)} = f_\theta^{(l)}(\mathbf{x}_{i,\text{pos}}^{(l)}); \mathbf{y}_{j,\text{neg}}^{(l)} = f_\theta^{(l)}(\mathbf{x}_{j,\text{neg}}^{(l)})$  # output [C, H, W]
    # calculate the goodness
     $G_{i,\text{pos}}^{(l)} = \frac{1}{C} \sum_c \mathbf{y}_{i,c,h,w,\text{pos}}^2$ ;  $G_{j,\text{neg}}^{(l)} = \frac{1}{C} \sum_c \mathbf{y}_{j,c,h,w,\text{neg}}^2$  # output [H, W]
    #  $\mathcal{L}_{\text{SCFF}}^{(l)}$  is initialized as 0 at each layer and is accumulated for each batch
     $\mathcal{L}_{\text{SCFF}}^{(l)} = \mathcal{L}_{\text{SCFF}}^{(l)} + \ell_{i,j}$ 
    # triangle method to transmit previous layer information to the next layer
     $\mathbf{y}_{i,\text{pos}}^{(l)} = \text{triangle}(\mathbf{y}_{i,\text{pos}}^{(l)}); \mathbf{y}_{j,\text{neg}}^{(l)} = \text{triangle}(\mathbf{y}_{j,\text{neg}}^{(l)})$ 
  end for
  Use optimizer to update network  $f_\theta^{(l)}$  to minimize  $\mathcal{L}_{\text{SCFF}}^{(l)}$ 
  # pooling operation to reduce the size of the feature maps
   $\mathbf{y}_{i,\text{pos}}^{(l)} = \text{POOL}(\mathbf{y}_{i,\text{pos}}^{(l)}); \mathbf{y}_{j,\text{neg}}^{(l)} = \text{POOL}(\mathbf{y}_{j,\text{neg}}^{(l)})$ 
end for
```

Appendix D Convolutional Layer architecture

In each layer, the input data is first processed by a convolutional layer, followed by either a "triangle" activation function or a ReLU activation, and then a pooling operation (as shown in the "CIFAR-10" and "STL-10" columns of Table D.1). It's important to note that the activations listed in Table D.1 are used solely for passing information to the next layer, whereas the activation function used for plasticity, i.e., during training, is consistently set as ReLU throughout all layers. In all experiments, the first layer had a width of 96 convolutional kernels, as described in [S2]. The number of kernels in subsequent layers was scaled by a factor of 4 relative to the previous layer.

To assess the performance of each layer, hidden neuronal activities are extracted from the pooling layer using an additional pooling operation (as shown in the "Layer's output" column of Table D.1) with the stride size matching the kernel size to reduce dimensionality. For the CIFAR-10 dataset, the final accuracy is calculated by aggregating the output neurons from all layers and using them as input to a linear classifier. For the STL-10 dataset, the final accuracy is derived by combining the output neurons from the last two layers (Layer 3 and Layer 4) and feeding them into a linear classifier. Other detailed architecture parameters are listed in the Table D.1.

Table D.1: Layer configurations across different datasets. The CIFAR-10 and STL-10 columns detail the structure of each layer, corresponding to the layer numbers listed in the first column. The "Layer's Output" column presents the additional pooling operation from the corresponding pooling layer, as indicated by the blue arrows, to form the input for the final linear classifier.

# layer	CIFAR-10		Layer's output	STL-10		Layer's output
1	5x5 Conv96 ¹			5x5 Conv96 ¹		
	Triangle			Triangle		
	4x4 MaxPool ³	→	2x2 AvgPool ⁵	4x4 MaxPool ³	→	4x4 AvgPool ⁵
2	3x3 Conv384 ²			3x3 Conv384 ²		
	Triangle			Triangle		
	4x4 MaxPool ³	→	2x2 AvgPool ⁵	4x4 MaxPool ³	→	4x4 AvgPool ⁵
3	3x3 Conv1536 ²			3x3 Conv1536 ²		
	ReLU			ReLU		
	2x2 AvgPool ⁴	→	2x2 AvgPool ⁵	4x4 MaxPool ³	→	4x4 AvgPool ⁵
4				3x3 Conv6144 ²		
				Triangle		
				2x2 MaxPool ⁴	→	3x3 MaxPool ⁵

¹With pad size of 2 and stride size of 1

²With pad size of 1 and stride size of 1

³With pad size of 1 and stride size of 2

⁴With pad size of 0 and stride size of 2

⁵With pad size of 0 and stride size the same as kernel size

Appendix E Recurrent Layer architecture

The bi-directional recurrent layer comprises two RNNs that process the sequence in opposite directions: one from the start to the end, and the other from the end to the start. Each RNN is composed of 500 hidden neurons. The input Mel-frequency Cepstral Coefficients (MFCC) feature at each time step is standardized before being fed into the hidden neurons. Additionally, the output hidden state at each time step is standardized before being passed to the next time step as the preceding state. The final output is generated by merging the outputs from the last time step of each direction, which is then used as input to the final linear classifier.

The MFCC features are derived from the audio waveform through a series of transformations that convert the raw audio signal into a representation that captures the phonetic content of speech, making it ideal for tasks like speech recognition. In our experiment, the audio is sampled at 16,000 Hz, and 39 MFCC coefficients are extracted.

Appendix F Hyperparameter optimization

We conducted a systematic investigation to determine the optimal set of hyperparameters for each hidden layer across all datasets.

For each dataset, we reserved a portion of the training set for validation purposes during hyperparameter tuning (20% for CIFAR-10 and STL-10, 10% for FSDD, and 10,000 samples from the MNIST dataset). Once the optimal hyperparameters were identified on the validation set, we retrained the model using the entire training and validation sets combined. The final test accuracy was then reported.

The classifier used in our experiments is a simple linear model trained directly on the outputs of the hidden layers (refer to Appendix D for details on retrieving the layer outputs), employing a dropout rate of 0.5 and no additional regularization terms (refer to Appendix G for the linear evaluation). We used a batch size of 100 for the MNIST, CIFAR-10, and STL-10 datasets, and a batch size of 64 for the FSDD dataset.

For data augmentation, we applied specific techniques based on the dataset: random horizontal flip for CIFAR-10, and padding followed by random cropping and horizontal flipping for STL-10.

```

1 # CIFAR-10:
2 transform = transforms.Compose([
3     transforms.RandomHorizontalFlip(),
4     transforms.ToTensor(),
5     transforms.Normalize((0.4914, 0.4822, 0.4465), (0.2023, 0.1994, 0.2010)),
6 ])

```

```

1 # STL-10:
2 transform = transforms.Compose([
3     transforms.RandomCrop(96, padding=4),
4     transforms.RandomHorizontalFlip(),
5     transforms.ToTensor(),
6     transforms.Normalize((0.4914, 0.4822, 0.4465), (0.2471, 0.2435, 0.2616)),
7 ])

```

The networks were trained using the Adam optimizer with weight decay, along with an Exponential Learning Rate Scheduler.

To search for the best hyperparameters, we utilized Optuna [S3]. The complete set of hyperparameters is detailed in Tables F.2, F.3 and F.4.

Table F.2: Hyper-parameters for CIFAR-10 dataset.

Layer	lr^1	Θ_{pos}	Θ_{neg}	λ	w_d^2	γ^3	Alg ⁴	Dropout ⁵	Epochs ⁶
1	0.01	0	1	0	0.0001	0.7		0.1	10
2	0.002	5	9	0.0007	0.0001	0.8	"1"	0.1	10
3	0.0002	6	10	0.0005	0.0003	1	"2"	0.2	25

¹ w_d : Learning rate of the AdamW optimizer.

² w_d : Weight decay coefficient of the AdamW optimizer.

³ γ : Multiplicative factor of learning rate decay (Exponential LR scheduler).

⁴ Alg: "1" represents Algorithm 1 and "2" represents Algorithm 2 in Appendix C.

⁵ Dropout: Dropout rate of the linear classifier.

⁶ Epochs: Maximum epochs needed to train.

Table F.3: Hyper-parameters for STL-10 dataset.

Layer	lr	Θ_{pos}	Θ_{neg}	λ	w_d	γ	Alg	Dropout	Epochs
1	0.026	0	2	0	0.001	0.99		0.4	8
2	0.003	5	8	0.0015	0.0003	0.8	"1"	0.4	10
3	0.001	6	8	0.005	0	0.99	"1"	0.4	10
4	0.0001	5	10	0.006	0.001	1	"2"	0.6	30

Table F.4: Hyper-parameters for FSDD datasets.

Layer	lr	Θ_{pos}	Θ_{neg}	λ	w_d	γ	Dropout	Epochs
1	2e-5	0	1	0.0075	0	0.7	0	10

Table F.5: Hyper-parameters for MNIST dataset.

Layer	lr	Θ_{pos}	Θ_{neg}	λ	w_d	γ	Dropout	Epochs
1	0.003	4	6	0.0001	1e-5	0.9	0.1	20
2	0.002	1	1	0	1e-5	0.6	0.2	20

F.1 Impact of λ , Θ_{pos} and Θ_{neg} on learning performance

The choice of hyperparameters such as λ , Θ_{pos} , and Θ_{neg} significantly impacts the learning performance. Table F.6 presents the test accuracies on the CIFAR-10 dataset when the penalty term is either included ($\lambda^{(2)} = 5e - 4$) or excluded ($\lambda^{(2)} = 0$) from the training loss, for various threshold values of Θ_{pos} during the training of the third convolutional layer. The results demonstrate that incorporating the penalty term consistently enhances training performance compared to omitting it.

Table F.7 further explores the test accuracies for different combinations of threshold values for $\Theta_{\text{pos}}^{(2)}$ and $\Theta_{\text{neg}}^{(2)}$ on the CIFAR-10 dataset. The results indicate that the highest accuracy is achieved when $\Theta_{\text{pos}}^{(2)}$ is slightly smaller than $\Theta_{\text{neg}}^{(2)}$.

Across all experiments, the optimal accuracy is typically reached within 25 epochs, with each reported accuracy representing the average of three runs using different random seeds.

Table F.6: Test accuracy (%) vs $\lambda^{(2)}$ for different $\Theta_{\text{pos}}^{(2)}$ on CIFAR-10 dataset. $\Theta_{\text{neg}}^{(2)} = 10$.

$\Theta_{\text{pos}}^{(2)}$	5	6	7	8	9
$\lambda^{(2)} = 0$	80.50	80.58	80.55	80.40	80.44
$\lambda^{(2)} = 5e - 4$	80.70	80.75	80.64	80.57	80.54

Table F.7: Test accuracy (%) vs $\Theta_{\text{pos}}^{(2)}$ and $\Theta_{\text{neg}}^{(2)}$ on CIFAR-10 dataset. $\lambda^{(2)} = 5e - 4$.

$\Theta_{\text{pos}}^{(2)}$	1	2	3	4	5	6	7	8	9
$\Theta_{\text{neg}}^{(2)} = 9$	80.61	80.55	80.65	80.64	80.62	80.64	80.63	80.46	80.44
$\Theta_{\text{neg}}^{(2)} = 10$	80.46	80.48	80.50	80.63	80.70	80.75	80.64	80.57	80.54

Appendix G Linear evaluation

We utilize the same linear classifier as detailed in [S2]. For vision tasks, the linear classifier employs a mini-batch size of 64 and is trained for 50 epochs on the MNIST, CIFAR-10, and for 100 epochs on the STL-10 dataset. The learning rate starts at 0.001 and is progressively halved at [20%, 35%, 50%, 60%, 70%, 80%, 90%] of the total epochs. Data augmentation is applied to enhance model robustness, with random horizontal flipping used for CIFAR-10, and random cropping and flipping used for STL-10. For FSDD dataset, the linear classifier employs a mini-batch size of 1 and is trained for 10 epochs. The learning rate starts at 0.0005 and is progressively halved at [20%, 35%, 50%, 60%, 70%, 80%, 90%] of the total epochs.

Appendix H Hierarchical representations

In Appendix H, we delve into the concept of hierarchical representations in convolutional neural networks (CNNs), specifically as learned by SCFF method on the STL-10 dataset. Fig. H.2 illustrates this concept by showcasing Class Activation Maps (CAMs) generated by a neural network after different stages of convolutional layers. The CAMs were calculated using the torchcam package [S4], which allows us to visualize the regions of an image that most significantly influence the network’s decision.

The progression of CAMs from Layer 1 to Layer 4 demonstrates how the network increasingly abstracts the features it learns from the input images. In Layer 1, the network focuses on low-level features such as edges and textures, while by Layer 4 (combined with layer 3), it has learned to identify more complex and abstract features that are crucial for accurate classification. Warmer colors in the CAMs (e.g., red and yellow) indicate areas of higher relevance, showing how the network’s focus shifts and intensifies on the most critical parts of the image as it moves through the layers. This hierarchical feature extraction underscores the effectiveness of the SCFF method in training CNNs, enabling them to capture the intricate details necessary for tasks like image recognition and classification.

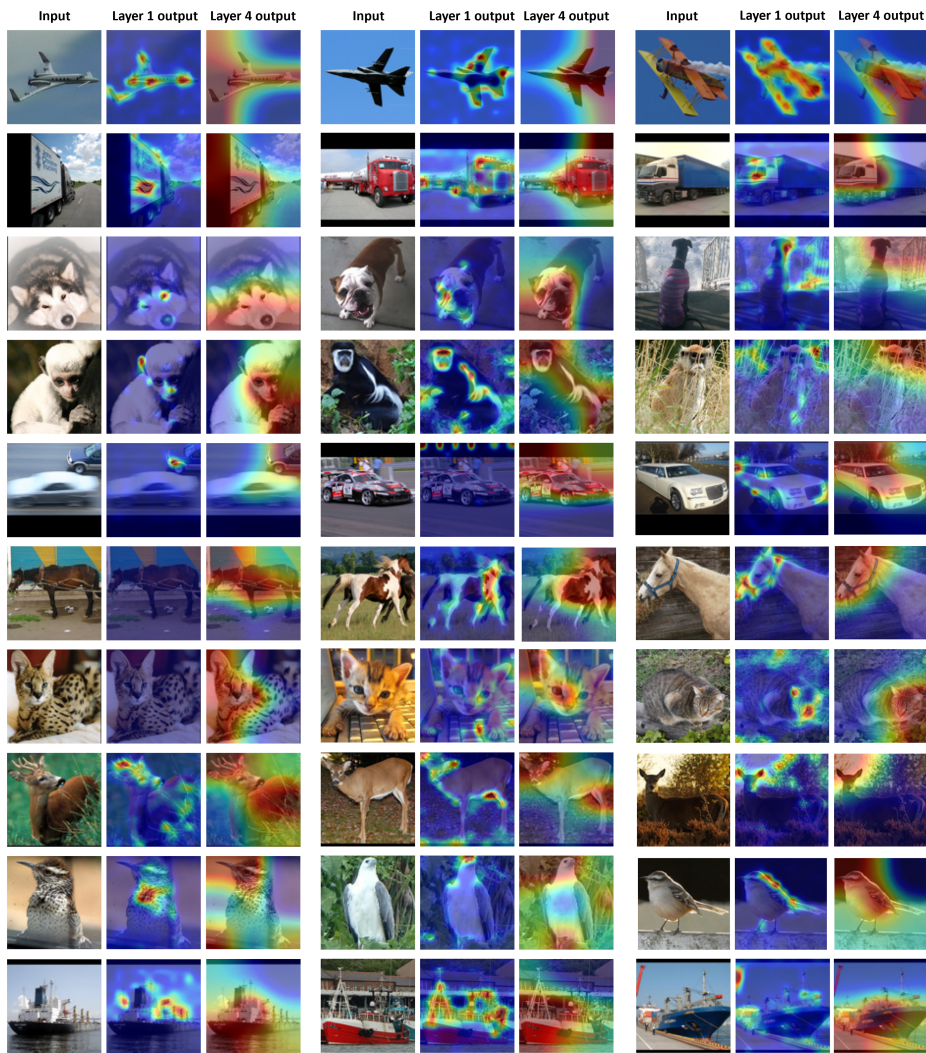


Fig. H.2: Indications for hierarchical representations learned by SCFF on STL-10 dataset. The "input" columns show the original input images to the network. The "Layer 1 output" and "Layer 4 output" columns display Class Activation Maps (CAMs) generated by the trained neural network after 1 convolutional layer and after 4 convolutional layers (combined with layer 3's features), respectively. These heatmaps highlight the regions in the image that contributed most strongly to the network's decision, with warmer colors (e.g., red and yellow) indicating areas of higher relevance. This progression demonstrates the increasingly abstract feature representations learned at deeper network layers.

References

- [S1] Kimin Lee, Sukmin Yun, Kibok Lee, Honglak Lee, Bo Li, and Jinwoo Shin. Robust inference via generative classifiers for handling noisy labels. In: International Conference on Machine Learning, pp. 3763–3772. PMLR, 2019.
- [S2] Adrien Journé, Hector Garcia Rodriguez, Qinghai Guo, and Timoleon Moraitis. Hebbian deep learning without feedback. arXiv preprint arXiv:2209.11883, 2022.
- [S3] Takuya Akiba, Shotaro Sano, Toshihiko Ohta, Takeru Yanase, and Masanori Koyama. Optuna: A next-generation hyperparameter optimization framework. In: Proceedings of the 25th ACM SIGKDD International Conference on Knowledge Discovery & Data Mining, pp. 2623–2631, 2019.
- [S4] François-Guillaume Fernandez. TorchCAM: Class activation explorer. GitHub, March 2020. <https://github.com/frgfm/torch-cam>